UNICA UNIVERSITÀ DEGLI STUDI DI CAGLIARI

Highlights

- The possibly systematic or accidental error source in density measurement by He-picnometry are mostly fluctuations in temperature, pollution (mainly moisture) of the sample and instrument, quantity, size and tortuosity of pores, time and mode of gas purging inside the instrument.
- Using an appropriate sequence of contiguous cycles, accuracy and precision of data can be optimized, thus excluding systematic errors.
- Regarding the degree of repeatability and reproducibility of density in the rock specimens, pulse mode shows a lower accuracy respect to flow mode, possibly due to random errors resulting from variations in temperature induced by adiabatic gas expansion. An optimization of the data accuracy can be achieved using 10-run cycles and computing the average value on the last seven. In this way, it is possible to reach an absolute deviations (or absolute errors) of $\pm$ 0.001 $\div$ 0.002, depending on the lithology.
- In the case of powder specimens the density data show greater accuracy then rock specimens, with differences of errors by almost one order of magnitude. Also in this case we suggest using two contiguous cycles characterised by time purge not too long (about 3 minutes) as they often cause a random error due to changes continuous of the structural setting of the powder, especially with very fine particle size (< 10 microns). If in the calculation of the mean value only the middle part of the values of the series is used, absolute deviations of the data around $\pm$ 0.001 can be reached.

Strategies for Helium pycnometry density measurements of welded ignimbritic rocks

***Columbu S.[1], Mulas M.[2], Mundula F.[1], Cioni R.[3]**

[1]*Department of Chemical and Geological Sciences, University of Cagliari - Cittadella universitaria, 09042 Monserrato (Cagliari), Italy - E-mail: columbus@unica.it - Phone number: +39 070 6757766*

[2]*Facultad de Ingeniería en Ciencias de la Tierra, Escuela Superior Politécnica del Litoral, ESPOL, Campus Gustavo Galindo Km 30.5 Vía Perimetral, P.O. Box 09-01-5863, Guayaquil, Ecuador*

[3]*Department of Earth Sciences, University of Florence, Via La Pira 4, 50121, Florence, Italy* *Corresponding author: Stefano Columbu

ABSTRACT

The helium pycnometer is commonly used to determine the real volume of rocks and powdered materials in order to calculate the bulk, real, solid density and porosity. Due to their specific textural features, welded ignimbritic rocks present a large range of porosity and pore structures, so that they need specific experimental setups for density and porosity measures. This study is aimed at recognizing possible sources of dispersion of real density measurements and to suggest a standard procedure for density analysis of ignimbritic products. Three lithofacies of Miocene ignimbrites from San Pietro Island (SW Sardinia, Italy), have been used to tune up a method using Helium pycnometer. The three samples have high bulk density and the determination of the solid fraction volumes of rock is often tricky, due to the presence of micropores and the high tortuosity of the porous network. We suggest that this is one of the main responsible of density data dispersion. Basing on a statistical study of the density data derived from different analytical strategies, we propose a specific procedure for determining density of welded ignimbritic rocks.

KEY WORDS: Helium pycnometry, Density, Porosity, Physical properties, Pyroclastic rocks, Welding, Ignimbrite, Precision, Accuracy.

1. Introduction

Determination of density and porosity of welded pyroclastic rocks is an important issue in order to define the rank of welding intensity [1] and hence the physical characteristics of these rocks [2]. Density determination is however not only important for the correct description of the rock texture and the processes of syn- or postdepositional welding, but also to characterize the mechanical features of these rocks that represent an important building material which is also present in many historical monuments worldwide [3-12]. Helium pycnometer allows the determination of these significant physical properties (density, porosity and volume) of bulk or powdered rock samples and other synthetic solid compounds. These physical properties, together with the mineralogical-petrographic features, are useful to define the characteristics of stone materials (*e.g.*, rocks and mortars) used in building construction or cultural heritage [13-18].

Due to the role played by the volatile phases in eruptive processes, volcanic rocks generally show a wide variability of porosity and, hence, density. In particular, density of pyroclastic rocks is mainly related to the

vesicularity of the constituting fragments and to the porosity of the deposit itself, on turn determined by grain size and shape distribution of the fragments, compaction, welding and syn- or post-depositional consolidation. Bulk density of ignimbritic rocks has been commonly related to their texture [19], welding degree [1] and componentry [20], which together define the lithofacies characteristics [21]. As these features are mainly affected by depositional and post-emplacement processes, the density is an important physical parameter largely used in ignimbrite studies [1, 20, 22-25].

Ignimbrite is a general term for the deposit of pyroclastic density currents, constituted by a poorly sorted ash matrix supporting pumice and lithic clasts [21]. The ash matrix is largely formed by glass shards, and by minor amounts of loose crystal and lithic fragments. Ignimbrite deposits may vary from completely loose to densely welded, in which glass particles are sintered and variably deformed and compacted. Welding degree is generally defined by orientation and deformation features of the rock and by their porosity [1, 22, 26]. Since density determination is of utmost importance in defining the rank of a welded ignimbrite and its mechanical properties, it is necessary to define a reference procedure for density measurements.

Basing on the results of the density analysis of three different ignimbritic lithofacies belonging to the Monte Ulmus Ignimbrite Unit, a Miocene deposit from the Sulcis volcanic district (Sardinia, Italy) [26-33], this paper is aimed at evaluating the main problems related to the measure of density of both undisturbed rocks and derived powdered materials. Due to the specific physical and textural characteristics of this type of rocks, a procedure for density measurements using Helium pycnometer is here presented and discussed, and some general suggestions for obtaining high precision and highly reproducible density measures are proposed.

2. Methods

2.1. Theory and system operation of the Helium pycnometer

The Helium pycnometer operation is based on the Archimede's principle of fluid displacement and on the Boyle's gas law. In reason of its small atomic dimension and of its ideal gas behaviour, helium can penetrate the finest pores ($<10^{-4}$ □m) so resulting in a hihgly accurate measure.

The instrument used for density determination is the Ultrapycnometer 1000 by Quantachrome Instruments. It consists of two cells separated by a solenoid valve (Fig. 1): the 'c' sample cell and the 'a' added cell with volume V_a (Fig. 1). Sample cell has three different cell volume possibilities, from 10 to 50 to 150 cm^3, which can be interchanged depending on the specimen size. The two cells are separated by a solenoid valve (Fig. 1). By opening this solenoid valve, the system is purged with helium, and is brought to ambient pressure P_a. The state is defined as $P_aV = n\,RT_a$, where '*n*' is the number of helium moles occupying the total volume V of two cells ($V_a + V_c$) at P_a, R is the gas constant (Reynold number) and T_a is the ambient temperature.

When a solid sample with volume V_p is placed in the cell at P_a, and the solenoid valve is closed, for the sample cell the equation can be written as:

$$P_a(V_c-V_p) = n_1\,RT_a \quad (1)$$

where n_1 represents the moles of gas in the sample cell at ambient pressure.

The state of added cell is represented by the following equation:

$$P_aV_a = n_a\,RT_a \quad (2)$$

where n_a represents the moles of gas in the added cell at ambient pressure.

After helium pressurization of the sample cell at P_2 (above ambient pressure) the new state of the sample cell is given by:

$$P_2(V_c-V_p) = n_2 RT_a \quad (3)$$

where n_2 represents the greater number of helium moles in the pressurised sample cell.

When the solenoid valve opens to connect the sample cell to the added cell, the pressure falls to a lower value P_3 and the equation of the system can be written as:

$$P_3(V_c-V_p+V_a) = (n_2 RT_a)+(n_a RT_a) \quad (4)$$

that substituting with equation (2) gives:

$$P_3(V_c-V_p+V_a) = (n_2 RT_a)+(P_a V_a) \quad (5).$$

Rearranging the above equations, we obtain:

$$V_p = V_c-[(P_a-P_3)V_a/(P_3-P_a)-(P_2-P_a)] = V_c+[V_a/(1-[(P_2-P_a)/(P_3-P_a)] \quad (6)$$ Since

all pressure values are normalized to P_a, equation (6) becomes:

$$V_p = (V_c+V_a)/[1-(P_2/P_3)] \quad (7)$$

that is the working equation to measure sample volume V_p.

The instrument calibrates V_a volume by performing two pressurizations, once with the sample cell empty (V_p = 0) and once with a calibration sphere of V_{cal} volume in the sample cell. The equations for these two conditions can be written as

$$V_p = 0 = V_c-V_a[1/[(P_2'/P_3')-1] \quad (8)$$

$$V_p = V_{cal} = V_c-V_a[1/[(P_2/P_3)-1] \quad (9)$$

Combining the equations (8) and (9) yields:

$$V_a = V_{cal}/[(1/(P_2'/P_3')-1]-[1/(P_2/P_3)-1] \quad (10)$$

The instrument calibrates V_c volume for a cell containing the sample holder and the calibration sphere. The equation $V_p = V_c+V_a/[1-(P_2/P_3)]$ is used, which can be written as:

$$V_p = V_{cal} = V_c+[V_a/(1-(P_2/P_3)] \quad (11.1) \text{ or } V_c = V_{cal}+[V_a/[(P_2/P_3)-1)] \quad (11.2)$$

2.2 Calibration and run parameters of Helium pycnometer

Calibration of the volume of the two cells is probably the most critical factor for obtaining a robust measure of the sample volume. Calibration of V_a value is made through two run sets. A blank run for the "added cell" under empty cell conditions is first made; the pycnometer is then purged for 1 minute and a second run is performed after inserting a calibration sphere in the added 'a' cell. This process continues until at least three consecutive measures reach a deviation respect to the preceding measure lower than 0.003%. If the required deviation is not obtained, calibration stops after 20 runs. In either case, the average of the last three runs is used to calculate the volume of V_a. Calibration is repeated for the sample cell (V_c).

Consequently, the operator has to handle some important run parameters: 1) the helium pressure (recommended range between 2 and 20 PSI, Pounds per Square Inch), 2) the equilibration time, that is the time needed to reach a pressure stabilization during the volume measure (short equilibration times may lead to a large variability of

density results), and 3) the purge mode (modality of gas release from the cells) which can be continuous (flow mode) or pulsating (pulse mode). For proper operation, the Helium pycnometer should work at constant ambient temperature, where the 18°C - 21°C range is the optimal temperature range. The minimum warm-up time to reach thermal equilibration should be of at least one hour.

Three main conditions have to be checked: 1) samples should be properly outgassed before starting a measure; 2) modality of the purge mode (pulse or flow mode) must be selected in relation to the sample lithology; 3) the number of runs which stabilize the measure of the sample volume.

According to data published by Quantachrome Instruments in Ultrapycnometer 1000 operation manual, the use of the large sample cell should imply deviations (respect to the measure) lower than ± 0.01%, that increase up to ± 0.03% with the medium and small sample cells as small variation of vapour pressure and deviation from thermal equilibrium have greater effect on small samples measure.

For an accurate sample measurement, the following points should be addressed to reduce data dispersion: i) avoiding vapour release form the sample (*e.g.*, due to presence of volatile impurities, moisture, alteration); ii) ensuring thermal equilibrium between cell and sample; iii) avoiding temperature differences between the gas tank and the pycnometer.

2.3 Analytical methods

Density measurements were performed on cubic-shaped rock specimens with a bulk volume varying between 2.43 and 4.10 cm^3, and on powdered rock samples with a mass of about 8 g.

The rock specimens were dried at 105 ± 5 °C and the dry mass (m_d) was determined. Later, the solid phase volume of powdered rock (V_S) and real volume of rock specimens (V_R) were determined with the Helium pycnometer, using the small sample cell (10 cm^3), where: $V_R = (V_S+V_{CP})$ and V_{CP} is the volume of closed pores. The bulk (total) volume of the undisturbed rock specimens (V_B) was then measured through the water absorption method, measuring the wet mass (m_w) of the sample after prolonged water immersion (three weeks) and the hydrostatic wet mass (m_{hw}) by mean a hydrostatic balance, as:

$$V_B = [(m_w-m_{hw})/\rho_{wTa}]$$

where: $V_B = (V_S+V_{OP}+V_{CP})$; V_{OP} is the volume of open pores; ρ_{wTa} is the water density at ambient temperature T_a (20°C) = 0.9982071 $g \cdot cm^{-3}$ [34].

Bulk density (ρ_B), real density (ρ_R) and solid density (ρ_S) were computed as: $\rho_B = m_d/V_B$; $\rho_R = m_d/V_R$; $\rho_S = m_d/V_S$.

2.4 Measurement strategy

The flow chart in Tab. 1 schematically shows the adopted measurement strategy. The different measures (runs) are organized in cycles and sequences. Each cycle starts with the instrument calibration and following purging of the cells of the pycnometer according to a defined procedure (for the pulse-mode, 10, 30 or 50 pulses; for the flow-mode, purging periods of 1, 3 or 5 minutes). After initial purging (for example with 10 pulses), helium is flowed into the instrument and the first measure (run) is performed. Gas is then extracted from the measuring cells (without repeating the initial purging procedure) that are then refilled with helium for the second run of

measurement. This is repeated to obtain 10 measurements, which together constitute a cycle. A new cycle of 10 runs is then initiated with a different purging setup (for example 30 pulses). The runs of this new cycle are then repeated to obtain 10 density measures. After this second cycle of the sequence, a third cycle is initiated with a new purging setup (for example 50 pulses) and measures repeated again for 10 times. These three cycles of measures constitute a sequence, which so consists of 30 density determinations; the variation trends of each cycle of measures are then analysed, in order to examine the convergence of the measures. For each cycle, an average value of density is also calculated and compared with the average values obtained for the other cycles of the same sequence. Varying the order of the three cycles of pulse mode measure and of the three cycles of flow mode measures, we test the accuracy of density data of six sequences: the 10-30-50, the 30-50-10, the 50-10-30 pulse mode sequences and the 1-3-5, the 3-5-1, the 5-1-3 flow mode sequences. The variability of the average values between the different sequences is then discussed.

In the discussion of the results, we will refer to:

1) *repeatability*, as the degree of concordance between density values of a 10-run series within a cycle, performed in a short period of time, at constant environmental conditions (*i.e.*, temperature, humidity). We assume as reference value (close to the true value) the average density of each ten runs cycle. Data dispersion has been quantified in terms of deviance (□), coefficient of variation (ν), variance (σ^2), standard deviation (σ), dispersion degree using the maximum range R and the interquartile range $\Delta_{Q1\text{-}Q3}$ (Tabs. 2, 3, 4), and in terms of maximum absolute (*a*E) and relative (*r*E%) errors (Tabs. 5, 6). The maximum absolute error data was calculated considering the farthest density value (*i.e.*, the maximum or minimum value for each cycle of ten runs) from the average density value of the measurement series.

2) *reproducibility*, as the goodness of fit of density data relative to different sequences. The reproducibility was evaluated comparing results of different sequences. The reproducibility has been evaluated comparing the different statistical parameters (*i.e.*, deviance, variance, standard deviation, density absolute value, kurtosis coefficient, Fischer index □₁, Tabs. 2, 3, 4), in three different experimental conditions (*i.e.*, with pulse numbers of 10, 30, 50, and with evacuation time of 1, 3, 5 minutes). The time between one and another series of tests has been about a week.

3. Petro-volcanological features of analysed ignimbritic rocks

Three welded rocks belonging to the Monte Ulmus Ignimbrite Unit (Sulcis Volcanic District, SW Sardinia, Italy [27, 30, 31] have been analysed. Monte Ulmus Ignimbrite is a rhyolitic, high-grade, locally rheomorphic, low-aspect-ratio ignimbrite [27]. Three main pyroclastic flow units (in the sense of Smith [33]), preceded by a basal fall-out deposit (F), have been distinguished, named A, B1 and B2 [27]. Unit A is a crystal-poor, densely welded ignimbrite. Unit B1 is a crystal-poor, fine grained, partially to densely welded, reddish tuff, while unit B2 is a partially to densely welded, light-grey to reddish, tuff. Both units B1 and B2 are characterized by the presence of black and white, cm- to dm-sized, highly flattened juvenile *fiammae*. Among these flow units, samples from three lithofacies with different petrophysical characteristics were selected and analysed:

1) Massive Vitric Tuff (MVT), consisting of black to reddish, massive, isotropic, vitric to partially argillified matrix, partially to densely welded. Mm- to cm-sized, dark- and light-coloured, platy, vitric *fiammae* have an

aspect ratio (length *vs*. thickness) largely variable between 3 and 30. Dispersed, broken to intact, free crystals of quartz and sanidine represent about 5 vol.% of the deposit. The rare, cm-sized lithic clasts are angular to sub-rounded. Oblate, cm-sized lithophysal cavities are ubiquitous. At the microscale, mm-sized glass shards generally display a well-developed parallel bedding, locally folded with a cm-sized wavelength. Glass shards in the MVT lithofacies are generally coalescent.

2) Massive lithofacies with vesicles (MvesT), represented by a reddish, eutaxitic, partially welded tuff. Cmsized black vitric *fiammae* are platy, with size varying from ash to lapilli. Mm-sized feldspar crystals are less than 5 vol.%; angular to slightly rounded lithic clasts, mainly represented by fragments of ignimbritic rocks, are present. Bladed, mm- to dm-sized, vesicles have their main axis parallel with the foliation planes. Micrometric glass shards are well oriented, parallel to the depositional plane.

3) Massive Isotropic breccia lithofacies (MIbrT), a very poorly sorted, matrix-supported, partially welded Tuff rich in lithic and juvenile blocks. Light-coloured, angular to sub-rounded pumice fragments may be larger than 50 cm in diameter, while blackish, platy, crystal-rich, sometimes deformed vitric spatters reach diameters up to 30 cm. Dm-sized, sub-rounded to angular lithic boulders are mixed together with large pumices and platy spatters. Sparse cm-sized lithophysal cavities are present. The analysed sample is representative of the breccia matrix.

4. Results

In the following paragraphs, the real density data of the three ignimbritic lithofacies (*i.e.*, MVT, MvesT, MIbrT) are presented according to the two different analytical procedures: pulse mode He-purge on rock samples (Tab. 2); flow mode He-purge on rock (Tab. 3) and on powdered samples of the same lithofacies (Tab. 4).

4.1 Pulse-mode measurements on the rock samples

The density values related to the three pulse-mode sequences are shown in Fig. 2 and Tab. 2. In the 10-30-50 sequence all the runs of the first cycle give the highest density values and show a nearly continuous decreasing trend along the cycle, particularly evident in the first three-four measures. Conversely, the density measurements of the following cycles show a quite flat trend, with slightly larger oscillations for the last (50pulses cycle). In general, the absolute value of density as determined in each cycle is different from the preceding one and decreasing from the first to the third cycle. The 30-50-10 sequence shows slightly higher values in the first cycle of 30 pulses, although without large variations within each cycle. The density values of each run of the last two cycles are practically indistinguishable. The 50-10-30 sequence shows again slightly higher values in the first cycle of measures (50 pulses), and a flat trend for the following cycles.

The variability of some selected statistical parameters (min-max, average, □ and interquartile range, $\square_{Q1\text{-}Q3,}$) is shown in Fig. 2b, d, f. In Tab. 2 the dispersion (R-variability) with respect to the median (m) are also reported. The interquartile difference ($\square_{Q1\text{-}Q3}$) represents an important measure of the data dispersion, including the central 50% of the observations. It is maximum for the first cycle of the 10-30-50 sequence, being however always lower than 5‰.

The mean value of real density (□□□of all the samples of each cycle □Tab. 2) shows a decreasing trend along the three cycles of each sequence (Fig. 2). The dispersion is highly variable among the cycles, with R between 3.64x10^{-2} □and 2 .50x10^{-3} □□he interquartile difference (□$_{Q1-Q3}$) varies according to R, showing values in the range 1.12x10^{-2} and 8x10^{-4}. The maximum dispersion is clearly related to the first cycle of the 10-30-50 sequence (Fig. 2, Tab. 2). The first cycle of the 10-30-50 sequence of sample MvesT shows the maximum dispersion respect to all the cycles of the three sequences. This could be related to the vesicular nature of the matrix of this sample, that possibly needs a more prolonged (higher number of purging pulses) purging procedure to be reliably evacuated and refilled.□

In general, in all the sequences, the second and third cycles show a narrower variability and interquartile difference than the first cycle; moreover, they show comparable mean density value.

4.2 Flow-mode measurements

4.2.1 Rock samples

Flow-mode measurements were made in a single sequence of three cycles with different gas-purge time duration (1, 3, 5 minutes). In the 1-min cycle the measured density shows a decreasing trend along the first three runs, while the following runs show a flat trend and a lower variability (Fig. 3). Conversely, the 3-min and 5-min cycles show flat trends for all the runs. Density measurements are largely more dispersed in the first (1-min) cycle, while the interquartile difference within each cycle is narrow, varying between 8x10^{-4} and 3.7x10^{-3} (Fig. 3, Tab. 3). The most important result, immediately evident from Fig. 3, is the higher density value measured in the first cycle (1 minute) of each sequence; this difference reaches a relative value (respect to the mean value) of about 1.4%, the highest difference measured for each cycle in each different mode or sequence.

4.2.2 Powdered samples

For calculating the porosity of a rock, the measure of the bulk density must be complemented with the measure of the density of the powdered rock, assuming that all the porosity has a size smaller than the average powder size, and that the porosity between the powder grains is easily accessed by the gas in the Hepycnometer measurements. For this reason, we have also tested reproducibility and precision for different sequence measurements with powders derived from the same three rock samples analysed above for bulk density.

Flow-mode measurements of powdered samples were made under flow purge mode according to the following three sequences: 1-3-5 minutes, 3-5-1 minutes, and 5-1-3 minutes.

Conversely from results on rock samples, powdered specimens show a nearly flat trend in all the cycles of runs (Fig. 4 and Tab. 4). This is especially true for the 1-3-5 sequence. The sequences related to sample MVesT show the larger differences between the density estimated in the different cycles, while in the sequences related to the other samples the results from the different cycles of each sequence are generally indistinguishable (Fig. 4). Unexpectedly, the different cycles often show a general tendency toward increasing density values from the initial to the last runs. All the samples show a poorly variable trend of average density in each cycle, with a narrow dispersion (Fig. 4). □he interquartile difference (□$_{Q1-Q3}$) is in the range 0.8-8x10^{-3}.

5. Discussion

The different procedures adopted and described above for the measurement of density of ignimbritic samples highlight some important issues regarding repeatability and reproducibility of data and can be used to propose a possible procedure for measuring this important property. In the following, we briefly discuss the differences resulting from the three procedures adopted for pulse-mode purge, and the differences observed in the results of flow *vs*. pulse modes.

5.1 Repeatability and reproducibility of measurements

5.1.1 Data from pulse- and flow-modes purge on rock samples

Data repeatability can be evaluated through the comparison of results obtained within each cycle of the three sequences (Fig. 2 and Tab. 2). For the three samples analysed, the larger variability is clearly associated to the 10-pulse cycles at the beginning of the 10-30-50 sequence (Figs. 2a, 2b), as highlighted by all the dispersion parameters (Fig. 5). In particular, all the 10-pulses cycles of this sequence show a continuously decreasing trend of density values from the first to the last measure of the cycle. This results in a lower repeatability of the first 10-pulse cycle respect to the 30 and 50-pulses cycles, as also evidenced by the larger standard deviation of the 10-pulses cycles (varying between 7.07×10^{-3} and 1.14×10^{-2}; Tab. 2) respect to the 30 and 50 pulses cycles (varying between 9.35×10^{-4} and 3.24×10^{-3}). Conversely, all the cycles of the 30-50-10 and 50-10-30 sequences (Figs. 2c, 2d, and Figs. 2e, 2f), present high repeatability, with values of standard deviation always lower than 2.42×10^{-3} (Tab. 2; Fig. 5). In all the three samples (MVT, MvesT and MIbrT), the 10-pulse cycles of the 10-30-50 sequence also show the most asymmetrical distribution of density measures, with values of Spearman skewness >1 (Tab. 2), according to the presence of few high values in the first three-four measurements of each cycle. As described above, this peculiar behaviour of the 10-pulses cycles can be observed only in the 10-30-50 sequence (Figs. 2a, 2b). Following these results, we suggest that, for establishing stable conditions of measures producing highly reproducible density results, several pulses of helium (50 or 30), pumping in and out from the instrument, are needed in the first runs of the sequence. The need of purging the sample-pycnometer system with several pulses could be related to the high tortuosity and low porosity features of the pore network of the analyses welded ignimbrites. These features could hinder the process of replacing the air hosted in the open porosity with helium during the measurement.

Reproducibility, the measure of the difference between results from the different sequences, can be best evaluated comparing results from the first cycles of the three sequences, or the final results of the three sequences (Fig. 5). The 10, 30 and 50-pulses cycles of the three sequences produced quite different results, both in terms of mean value and of internal variability of the 10 density values measured in each run (Tab. 2; Fig. 5).

An interesting result is that, whatever the number of purging pulses, the first cycles of each sequence always return density values higher than the following cycles, with differences between the mean values generally within the standard deviation.

Finally, when comparing the values of mean density resulting from the last cycle of each sequence (and for each sample), we observe a substantial convergence of all the results, with a very large reproducibility of the data as

all the mean values are practically indistinguishable one from the other within 1σ (the maximum relative difference between the measured values for each sample being not higher than 2.5 x 10^{-3}; data from Tab. 2).
Reproducibility could be also tested by comparing the results of the three pulse-mode sequences with those of the flow-mode 1-3-5 sequence (Figs. 3a, 3b, 5; Tab. 3). Comparison of results of the 1-min cycle at the onset of the sequence with the results of the firsts cycles of the pulse-mode sequences suggests a good concordance of data with the results from 30 and 50-pulses cycles. However, a clear sample-dependence of data appears when looking at data of MIbrT sample. Conversely, the mean density values resulting from the final cycle of all the sequences (both pulse- or flow-mode) on all the measured samples are all indistinguishable and within
1□.
Data reproducibility varies within the three samples in dependence of their different petrophysical characteristics. Figs. 6a shows a positive correlation between the dispersion parameters and the bulk density (ρ_B) of the three analysed lithofacies. This clear correlation (*e.g.*, the deviance: $R^2 = 0.99823$, Fig. 6a) highlights that the reproducibility degree of density measurements is positively correlated with the density
(and hence welding degree) of these ignimbrites, as also evidenced by the average values of the Δ_{Q1-Q3} (Fig. 6b), the variation range (R; Tabs. 2, 3) and the maximum absolute errors (Tabs. 5, 6).

5.1.2 Data from flow-mode purge on powders

Due to their different composition, the three ignimbritic samples show different solid density values. The sample from MIbrT lithofacies, characterised by a high amount of lithic fragments and a low amount of volcanic glass matrix, shows the lowest values of dispersion parameters (Figs. 4a-f, 7). The MvesT and the MVT samples, which show comparable componentry and lithologic features, shows larger dispersion values with respect to the MIbrT.
Except some cases sequences (*e.g.*, 5-1-3 in the MVT, 1-3-5 in the MvesT and 3-5-1 MVT), all other sequences performed with the purge-mode show lowest values of dispersion parameters in the last cycle. There is no correlation between the length of purge time and the values of statistical parameters (variance, standard deviation, etc.) and the accuracy of the data. The solid density absolute values of the three powdered samples, except for a few cases, are most commonly higher in the first cycle of each sequence, showing the same behaviour shown in the case of rock specimens.
The substantial difference in the powdered rock is that it does not detect a clear instrumental drift in the three cycles of the three sequences (Fig. 7), with the absence of systematic errors in the solid volume values, which leads in the case of rock specimens to a progressive increase of the real volume value (and so a decrease of real density), especially in the first cycle (Fig. 5). Indeed, as shown by the deviance, it seems that the values tend to grow in the progression of ten runs, or, in other cases, to show constant average deviations around the mean.

5.2 Systematic error and progression data

Solid density results (on powders) show a slight, continuous increasing trend of the density values within each cycle. Conversely, both in the case of pulse and flow modes measures, undisturbed rock specimens show a general decrease of real density data from the first to the final runs of each cycle, which is particularly evident

during the first three runs (Figs. 2, 3). The steepness of this decreasing trend is clear in the first cycle of each sequence, but to a lesser extent it can be observed also in the second and third cycles, even independently from the sequence. We suggest that this decreasing trend of density data highlights a systematic error which could be due: 1) a temperature drift related to thermal disequilibrium between the pycnometer and environmental conditions, due, on the one side, to the heating of the instrument during its use and, on the other side, to the cooling of the instrument caused by the various adiabatic expansion cycles of the numerous runs on an increase of the instrument temperature during its operation or on the decrease of temperature caused by adiabatic expansion during the run cycles, 2) the presence of pollutants (especially humidity) within the smaller sub-micrometric pores of the rock specimen and in the internal system of the pycnometer.

To better understand this behaviour, in the Figs. 8a, 8b, 8c, flow-mode density data of the 1-3-5 sequence have been plotted as the average (and the relative standard deviations) calculated on a decreasing number of runs, from ten runs [$\mu_{(i = 1\text{-}10)}$] to three runs [$\mu_{(i = 7\text{-}10)}$]. The relative standard deviation, also plotted on the same diagram, decreases with decreasing the run number on which the average is calculated. it is recommended to calculate the density counting the last seven (or eight) runs, thus neglecting the first three readings of the instrument. This is particularly evident in the case of 3 minutes (Fig. 8b, c).

5.3 Procedure recommendations *5.3.1*

Undisturbed rock samples

Results showed a comparable degree of repeatability between the two purge modes (pulse *vs.* flow). Conversely, significant differences in the reproducibility is evident among the different sequences when considering the number of pulses or length of the flow. Dispersion of real density data shows a clear positive correlation with the bulk density and with the welding degree of the lithofacies. The increase of the welding is commonly related to a progressive decrease of porosity in terms of vesicle size and shape and to an increase of the tortuosity of the pore network. Thus, these textural features are possibly the cause of an increase of the stabilization time of the helium within the circuit/cells of the pycnometer possibly generating a greater dispersion of output data.

Considering the third cycle of the pulse mode 10-30-50 sequence and of the 1-3-5 sequence that show, overall, low dispersion of density data (Tab. 5), the pulse-mode results show a lower degree of accuracy (with maximum standard deviations from ± 0.00159 for MIbrT, to ± 0.00432 for MvesT, to ± 0.00454 for MVT; Tab. 2) with respect to the flow-mode (from ± 0.000844 for MIbrT, to ± 0.00275 of MvesT, to ± 0.00251 of MVT; Tab. 3). We suggest that the process of purging the system with repeated pulses could produce drops in temperature, as a result of the repeated adiabatic expansions. We suggest to use the purge pulse mode only in the case of pycnometers provided by a system of stabilization of temperature.

It has been shown that, regardless to the purge mode and sequences, the first cycle of a sequence shows higher dispersion values (Fig. 5) than the subsequent cycles (with a maximum deviation in the pulse purge from ± 0.0129 for MVT, to ± 0.0167 for MIbrT, to ± 0.0281 for MvesT, Tab. 2; in the flow purge from ± 0.0115 for MvesT, to ± 0.0119 for MVT, to 0.0121 for MIbrT, Tab. 3). The low repeatability of the first cycle is generally associated to an overestimation of the density that can be related to an underestimation of the specimen volume. Finally, we recommend to extract density data from the second of two flow-mode cycles (without opening the

system), where the first cycle must have a purge time of 3÷5 minutes and the later must have a purge time of 1-3 minutes. It is also shown that by selecting a portion of the population of values (*e.g.*, the last seven of ten runs) in the calculation of mean, the standard deviation decreases significantly (sometime almost an order of magnitude; Fig. 8).

5.3.2 Powdered rock samples

The results on powdered specimens and rock specimens show a similar behaviour in term of reproducibility (Fig. 7). Conversely a different repeatability degree within the ten runs cycle has been observed; the maximum deviations on powdered samples are lower than those on rock specimens (from ± 0.0014% for MIbrT to ± 0.0094% for MvesT, Tab. 4), and density data tend to remain around the average solid density values or show a slight increase.

The difference is possibly due to the different distribution and type of porosity in the two kind of sample: in rock specimens the porous network consists of open and closed porosity with smaller pores with respect to the powdered samples, characterized by a higher tortuosity which slows down the flow of helium. Moreover, if the grains are finer than 10 microns, they could be retained by the pre-filter valve, and resulting in error in the volume measure. The process of helium diffusion within the powder could move the grains, resulting in an increase of the equilibrium time and possibly involving some variability of volume measures. Therefore, in the case of powdered samples, a prolonged purge time gives greater standard deviations, as confirmed by the negative correlation between data accuracy and purge time (Figs. 4, 7). In fact, the absolute error reduces in the case of 1minute cycle (Tab. 6). Possibly, the helium flushing into the sample cell during the analysis could be able to change the geometric arrangement of granules. As tested by unpublished experimental data, a greater compaction degree of powders can improve data accuracy. Thus, in order to prevent the movement of powder grains during analysis and to minimize the standard deviation, we suggest to mechanically compact the samples during the preparation of specimens.

In the case of powders, as a longer purge time involves a decrease of accuracy (Tab. 6), we suggest to extract the density data from the second of two contiguous cycles (without opening the system), and to calculate the average value of an intermediate data population (*e.g.*, in the case of 10 runs discarding the first 3 runs and the last 2 runs of each series). We also suggest to use a 3 minutes purge time in the first cycle and a 1 minute purge time in the second cycle. A further suggestion is to avoid the use of very fine grain of powder (< 10 microns) that can pass through the filter (Fig. 1) and deposit inside the circuit, thereby affecting the determination of the solid volume.

6. Conclusions

The data have identified accidental and systematic errors in the density pycnometer analysis of welded ignimbrites. The repeatability degree of instrument depends by various factors that may affect the data accuracy and precision. The main factors that can produce an error source (either systematic or accidental) are mostly fluctuations in temperature, pollution of the sample (principally moisture) and of the instrument, the physical characteristics of the porous rock network (*e.g.*, quantity and size of close and open porosity, complexity of the tortuosity). The repeatability is also affected by the purge time and mode of gas purging inside the instrument

during the first steps of the analysis. Using an appropriate sequence of contiguous cycles, accuracy and precision of data can be optimized, thus excluding systematic errors. The results show that in the first cycle, regardless of the purge time (or pulses), the values of density and standard deviations are higher compared to the second and the third cycles.

Density of rock specimens could be derived both from flow and pulse-mode, as we observed only small differences in the degree of repeatability and reproducibility. However, pulse mode shows a lower accuracy respect to flow mode, possibly due to random errors resulting from variations in temperature induced by adiabatic gas expansion. In both the purge modes, the measurements obtained from the second cycle of two, with a minimum purge time of the first cycle of 3 minutes (or 30 pulse) and at least 1 minute (or 10 pulses) in the second cycle, are more accurate. An optimization of the data accuracy can be achieved using 10-run cycles and computing the average value on the last seven. In this way, it is possible to reach an absolute deviations (or absolute errors) of ± 0.001 ÷ 0.002, depending on the lithology. Following this procedure, the real density (g cm^{-3}) of these volcanic rocks could be determined to the third decimal digit.

In the case of powder specimens the density data show greater accuracy then rock specimens, with differences of errors by almost one order of magnitude. Also in this case we suggest using two contiguous cycles characterised by time purge not too long (about 3 minutes) as they often cause a random error due to changes continuous of the structural setting of the powder, especially with very fine particle size (< 10 microns). If in the calculation of the mean value only the middle part of the values of the series is used, absolute deviations of the data around ± 0.001 can be reached.

References

[1] S.L. Quane, J.K. Russell, Ranking welding intensity in pyroclastic deposits, Bulletin of Volcanology. 67 (2) (2005) 129 – 143.

[2] S. Columbu, A. Gioncada, M. Lezzerini, M. Marchi, Hydric dilatation of ignimbritic stones used in the church of Santa Maria di Otti (Oschiri, northern Sardinia, Italy), Ital. J. Geosci. 133 (2014) 149 – 160.

[3] C. Stanislao, C. Rispoli, G. Vola, P. Cappelletti, V. Morra, M. De Gennaro, Contribution to the knowledge of ancient Roman seawater concretes: Phlegrean pozzolan adopted in the construction of the harbour at Soli–Pompeiopolis (Mersin, Turkey), Periodico di Mineralogia. 80 (3) (2011) 471 – 488.

[4] S. Columbu, Petrographic and geochemical investigations on the volcanic rocks used in the Punic–Roman archaeological site of Nora (Sardinia, Italy), Environmental Earth Science. 77 (16) (2018) 577.

[5] G. Verdiani, S. Columbu, E. Stone, An archive for the Sardinia monumental witnesses, Lecture Notes in Computer Science. 6436 (2010) 356 – 372.

[6] S. Columbu, M. Palomba, F. Sitzia, M.R. Murgia, Geochemical, mineral-petrographic and physical–mechanical characterization of stones and mortars from the Romanesque Saccargia Basilica (Sardinia, Italy) to define their origin and alteration, Italian Journal of Geosciences. 137 (3) (2018) 369 – 395.

[7] A. Binal, Prediction of mechanical properties of non-welded and moderately welded ignimbrite using physical properties, ultrasonic pulse velocity, and point load index tests, Q. J. Eng. Geo. and Hydro. 42 (2009) 107 – 122.

[8] S. Columbu, G. Verdiani, Digital Survey and Material Analysis Strategies for Documenting, Monitoring and Study the Romanesque Churches in Sardinia, Italy, Lecture Notes in Computer Science, Springer. 8740 (2014) 446 – 453.

[9] S. Columbu, G. Piras, F. Sitzia, S. Pagnotta, S. Raneri, S. Legnaioli, V. Palleschi, M. Lezzerini, M. Giamello, Petrographic and mineralogical characterization of volcanic rocks and surface-depositions on Romanesque monuments, Mediterranean Archaeology and Archaeometry. 18 (5) (2018) 37 – 64.

[10] G. Heiken, Tuffs: their properties, uses, hydrology, and resources, Geological Society of America. 408 (2006).

[11] S. Columbu, Provenance and alteration of pyroclastic rocks from the Romanesque Churches of Logudoro (north Sardinia, Italy) using a petrographic and geochemical statistical approach, Applied Physics A: Materials Science and Processing. 123 (3) (2017) 165.

[12] S. Columbu, C. Lisci, F. Sitzia, G. Lorenzetti, M. Lezzerini, S. Pagnotta, S. Raneri, S. Legnaioli, V. Palleschi, G. Gallello, B. Adembri, Mineralogical, petrographic and physical-mechanical study of Roman construction materials from the Maritime Theatre of Hadrian's Villa (Rome, Italy), Measurement: Journal of the International Measurement Confederation. 127 (2018) 264 – 276.

[13] S. Columbu, A.M. Garau, Mineralogical, petrographic and chemical analysis of geomaterials used in the mortars of Roman Nora theatre (south Sardinia, Italy), Italian Journal of Geosciences. 136 (2017) 238 – 262.

[14] C. Buosi, S. Columbu, G. Ennas, P. Pittau, G.G. Scanu, Mineralogical, Petrographic, and Physical Investigations on Fossiliferous Middle Jurassic Sandstones from Central Sardinia (Italy) to Define Their Alteration and Experimental Consolidation, Geoheritage. 11 (2018). https://doi.org/10.1007/s12371-018-0326-8.

[15] S. Columbu, C. Lisci, F. Sitzia, G. Buccellato, Physical–mechanical consolidation and protection of Miocenic limestone used on Mediterranean historical monuments: the case study of Pietra Cantone (southern Sardinia, Italy), Environmental Earth Sciences. 76 (4) (2017) 148.

[16] M. Lezzerini, S. Raneri, S. Pagnotta, S. Columbu, G. Gallello, Archaeometric study of mortars from the Pisa's Cathedral Square (Italy), Measurement: Journal of the International Measurement Confederation. 126 (2018) 322 – 331.

[17] S. Columbu, M. Palomba, F. Sitzia, M.R. Murgia, Geochemical, mineral-petrographic and physical-mechanical characterization of stones and mortars from the Romanesque Saccargia Basilica (Sardinia, Italy) to define their origin and alteration, Italian Journal of Geosciences. 137 (3) (2018) 369 – 395.

[18] S. Columbu, F. Sitzia, G. Ennas, The ancient pozzolanic mortars and concretes of Heliocaminus baths in Hadrian's Villa (Tivoli, Italy), Archaeol Anthropol Sci. 9 (4) (2017) 523 – 553.

[19] A.L. Grunder, D. Laporte, T.H. Druitt, Experimental and textural investigation of welding: effects of compaction, sintering, and vapor-phase crystallization in the rhyolitic Rattlesnake Tuff, J. Volcanol. Geotherm. Res. 142 (1–2) (2005) 89 – 104.

[20] G.A. Mahood, Pyroclastic rocks and calderas associated with strongly peralkaline volcanic rocks, Journal of Geophysical Research. 89 (1984) 8540 – 8552. https://doi.org/10.1029/JB089iB10p08540.

[21] M.J. Branney, P. Kokelaar, Pyroclastic density currents and the sedimentation of ignimbrites, Geological Society of London. (2002).

[22] A.L. Grunder, J.K. Russell, Welding processes in volcanology: insights from field, experimental, and modeling studies, J. Volcanol. Geotherm. Res. 142 (2005) 1 – 9.

[23] M. J. Streck, A.L. Grunder, Crystallization and welding variations in a widespread ignimbrite sheet; the Rattlesnake Tuff, eastern Oregon, USA, Bulletin of Volcanology. 57 (3) (1995) 151 – 169.

[24] G.P.L. Walker, Ignimbrite types and ignimbrite problems, J. Volcanol. Geotherm. Res. 17 (1983) 65 – 88.

[25] F. Mundula, R. Cioni, M. Mulas, Rheomorphic diapirs in densely welded ignimbrites: The Serra di Paringianu ignimbrite of Sardinia, Italy, J. Volcanol. Geotherm. Res. 258 (2013) 12-23.

[26] F. Mundula, R. Cioni, R. Rizzo, Welded ignimbrite of San Pietro Island (Sardinia, Italy): a proposal of micro facies nomenclature, Boll. Soc. Geol. It. 128 (2009) 615 – 627.

[27] M. Mulas, R. Cioni, F. Mundula, Stratigraphy of the rheomorphic, densely welded, Monte Ulmus ignimbrite (SW Sardinia, Italy), Acta vulcanologica. (2012) 17 – 26.

[28] A. Assorgia, A. Fadda, D.G. Torrente, V. Morra, L. Ottelli, F.A. Secchi, Risultati preliminari sullo studio delle successioni vulcaniche terziarie del Sulcis (Sardegna sudoccidentale), 75° Congr. Naz. S.G.I., Milano. (1990) 3 – 5.

[29] A. Assorgia, A. Fadda, D.G. Torrente, V. Morra, L. Ottelli, F.A Secchi, Le successioni ignimbritiche terziarie del Sulcis (Sardegna sud-occidentale), Mem. Soc. Geol. It. 45 (1990) 951 – 963.

[30] R. Cioni, L. Salaro, L. Pioli, The Cenozoic volcanism of San Pietro Island (Sardinia, Italy), Rendiconti Seminario Facoltà Scienze Università Cagliari. 71 (2) (2001) 149 – 163.

[31] L. Lecca, R. Lonis, S. Luxoro, F. Melis, F. Secchi, P. Brotzu, Oligo-Miocene volcanic sequences and rifting stages in Sardinia, Periodico di Mineralogia. 66 (1997) 7 – 61.

[32] V. Morra, F.A. Secchi, A. Assorgia, Petrogenetic significance of peralkaline rocks from Cenozoic calcalkaline volcanism from SW Sardinia, Italy. Chem. Geol. 118 (1994) 109 – 142.

[33] R.L. Smith, Zones and zonal variations in welded ash-flows, U.S. Geol. Surv. Prof. Pap. 354 (1960) 149 – 158.

[34] R.C. Weast, Handbook of Chemistry & Physics, 53rd ed., CRC Press,Cleveland, Ohio (1972), pp. E183 – E184.

Captions of Figures and Tables

Figure 1. Flow diagram of Ultrapycnometer 1000 by Quantachrome Instruments.

Figure 2. (a, c, e) Real density series of ten runs of MVT, MvesT, MIbrT rock specimens of three number of pulse purge mode with following three pulse number sequences: (10, 30, 50), (30, 50, 10), (50, 10, 30).
(b, d, f) Box-and-whisker (boxplot) with main statistic parameters of real density series of 10 runs with pulse purge. On the x-axis the each cases pulse sequences (10, 30, 50), (30, 50, 10), (50, 10, 30) are reported. On the y-axis, for each case (10, 30, 50 pulses) are reported: the range (black vertical continuous line) between the minimum and maximum of absolute real density values; the mean values of real density (horizontal dot line); the interquartile difference $\square_{Q1\text{-}Q3}$ (empty boxplot), where Q_1 and Q_3 are the 1° and 3° quartile (inferior horizontal black line, superior horizontal black line, respectively).

Figure 3. (a) Real density series of ten runs of MVT, MvesT and MIbrT rock specimens of three number of flow purge with the following minute sequence: (1, 3, 5). Symbols as in Fig. 2.
(b) Box-and-whisker (boxplot) with main statistic parameters of real density series of 10 runs (with flow purge). On the x-axis the case pulse sequence (1, 3, 5) is reported. On the y-axis, for each case (1, 3, 5 flow minutes) are reported: the range (black vertical continuous line) between the minimum and maximum of absolute real density values; the mean values of real density (horizontal dot line); the interquartile difference $\square_{Q1\text{-}Q3}$ (empty boxplot), where Q_1 and Q_3 are the 1° and 3° quartile (inferior horizontal black line, superior horizontal black line, respectively).

Figure 4. (a, c, e) Solid density series of ten runs of MVT, MvesT and MIbrT rock powdered specimens of three number of flow purge with following three sequences: (1, 3, 5), (3, 5, 1), (5, 1, 3).
(b, d, f) Box-and-whisker (boxplot) with main statistic parameters of real density series of 10 runs with flow purge. On the x-axis the each cases pulse sequences (1, 3, 5), (3, 5, 1), (5, 1, 3) are reported. On the y-axis, for each case (1, 3, 5 flow minutes) are reported: the range (black vertical continuous line) between the minimum and maximum of absolute real density values; the mean values of real density (horizontal dot line); the interquartile difference $\square_{Q1\text{-}Q3}$ (empty boxplot), where Q_1 and Q_3 are the 1° and 3° quartile (inferior horizontal black line, superior horizontal black line, respectively).

Figure 5. Deviance, variance, variation coefficient and standard deviation of real density series of 10 determinations for MVT, MvesT and MIbrT rock specimens on the two purge modes: pulse for first three rows on the (10, 30, 50), (30, 50, 10), (50, 10, 30) sequences; flow for four row on the (1, 3, 5) sequence.

Figure 6. (a) Means of deviance, variance, variation coefficient and standard deviation of real density series of MVT, MvesT and MIbrT lithofacies, calculated on value means of six rock specimens on flow purge time of 1, 3, 5 minutes. (b) Means of $\square_{Q1\text{-}Q3}$ of real density series calculated on value means of six rock specimens on time flow purge of 1, 3, 5 minutes.

Figure 7. Deviance, variance, variation coefficient and standard deviation of solid density series of 10 determinations for MVT, MvesT and MIbrT powdered specimens on the flow purge in the following three minutes sequences: (1, 3, 5), (3, 5, 1), (5, 1, 3).

Figure 8. Real density and relative standard deviation of MVT (a), MvesT (b) and MIbrT (c) rock specimens, calculated in the 1st sequences (1, 3, 5 minutes) of the flow purge on the value series with decrease number of runs with means from □□(i=1÷10) con *n* = 10, to □ (i=7÷10) con *n* = 3, where □ is mean of run values and *n* the number of computed runs.

Table 1. Measurement strategy used for the sample analysis, organized in ten runs for each performed cycle with pulses or flow purge mode, and three cycles for each performed sequence with three different pulse numbers (10, 30, 50) or flow time (1, 3, 5 minutes). n.d. = not determined.

Table 2. Real density values on ten run cycles and main statistic parameters of MVT, MvesT and MIbrT rock specimens determined on pulse purge mode with sequence of (10, 30, 50), (30, 10, 50) and (50, 10, 30) pulses. Legend: □□= average of real density; □ = standard deviation; □² = variance; □□= deviance; R = maximum range of real density; □ = variation coefficient; C = confidence interval; Q_1 = 1° quartile of statistic distribution of ten values; Q_3 = 3° quartile; $□_{Q3-Q1}$ = difference between 1st and 3rd quartile; m = median (Q_2); k = kurtosis coefficient of Pearson; □ = asymmetry index of Fischer (or coefficient of skewness).

Table 3. Real density values on ten run series and main statistic parameters of MVT, MvesT and MIbrT rock specimens determined on flow purge mode with sequence of (1, 3, 5) minutes. Legend as in Table 2.

Table 4. Solid density values on ten run series and main statistic parameters of MVT, MvesT and MIbrT powdered specimens determined on flow purge mode with sequence of (1, 3, 5), (3, 5, 1) and (5, 1, 3) minutes. Legend as in Table 2.

Table 5. Absolute error (*a*E) and relative error (*r*E %) of real density values of MVT, MvesT and MIbrT rock specimens determined with helium pycnometry with pulse purge mode on the three sequences: (10, 30, 50), (30, 50, 10) and (50, 10, 30) pulses, and with flow purge mode on the sequence (1, 3, 5) minutes. Absolute error is calculated as difference between the maximum (or minimum) value and the average value (that is considered as the true density value) of ten run measurements.

Table 6. Absolute error (*a*E) and relative error (*r*E %) of solid density values of MVT, MvesT and MIbrT powdered specimens determined with Helium pycnometry with flow purge mode on the three sequences: (1, 3, 5), (3, 5, 1) and (5, 1, 3) minutes.

Figure 1

Click here to access/download;Figure(s);Fig.1.jp

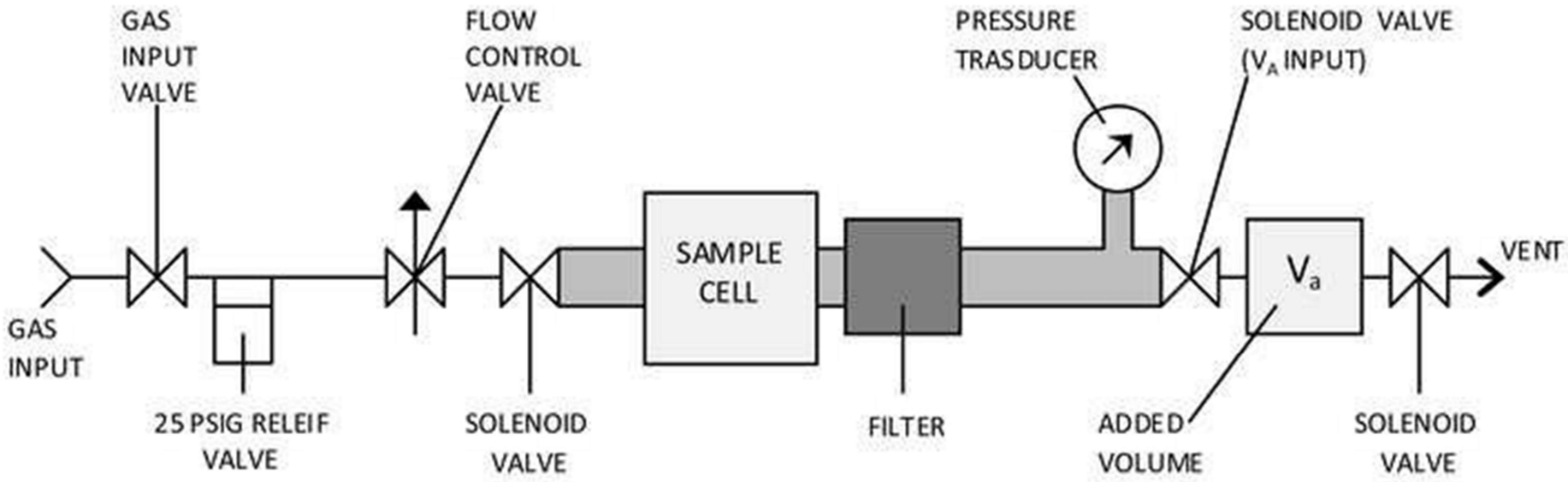

Figure 2

g

Click here to access/download;Figure(s);Fig.2.jp

Figure 3

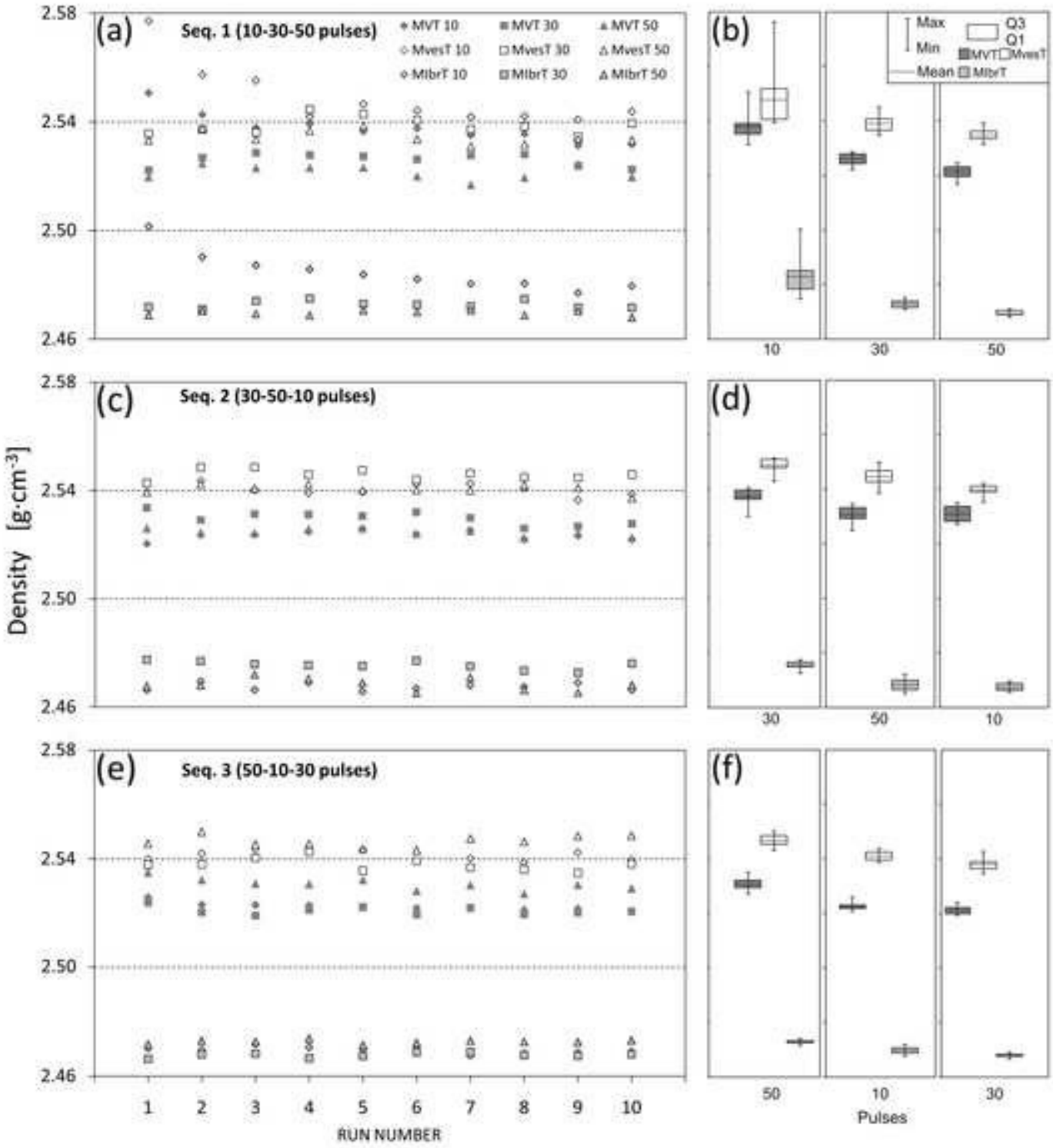
(a)
Seq. 1 (10-30-50 pulses)
MVT 10
MVT 30
MVT 50
MvesT 10
MvesT 30
MvesT 50
MIbrT 10
MIbrT 30
MIbrT 50
(b)
Max
Min
Mean
Q3
Q1
MVT
MvesT
MIbrT
10
30
50
(c)
Seq. 2 (30-50-10 pulses)
(d)
30
50
10
(e)
Seq. 3 (50-10-30 pulses)
(f)
50
10
30
Pulses
Density [g·cm-3]
2.58
2.54
2.50
2.46
1
2
3
4
5
6
7
8
9
10
RUN NUMBER

Figure 4

g

Click here to access/download;Figure(s);Fig.3.jp

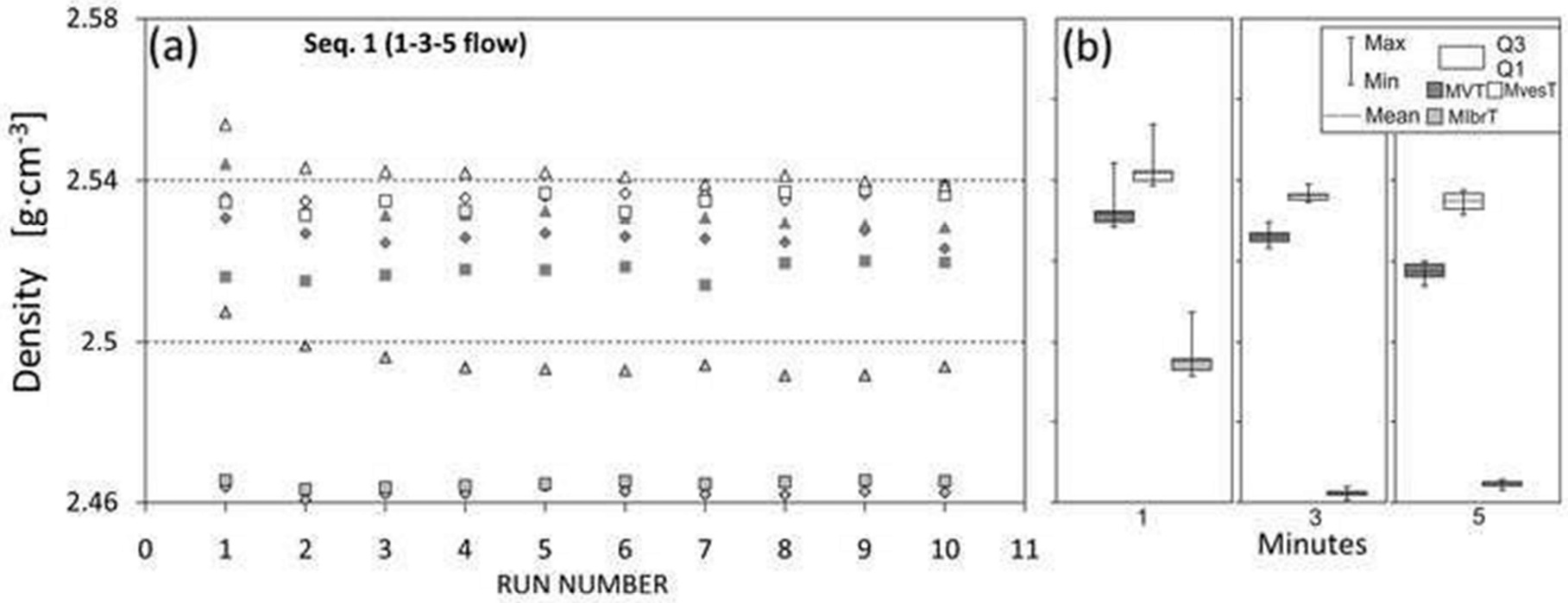

Figure 5

g

Click here to access/download;Figure(s);Fig.4.jp

Figure 6

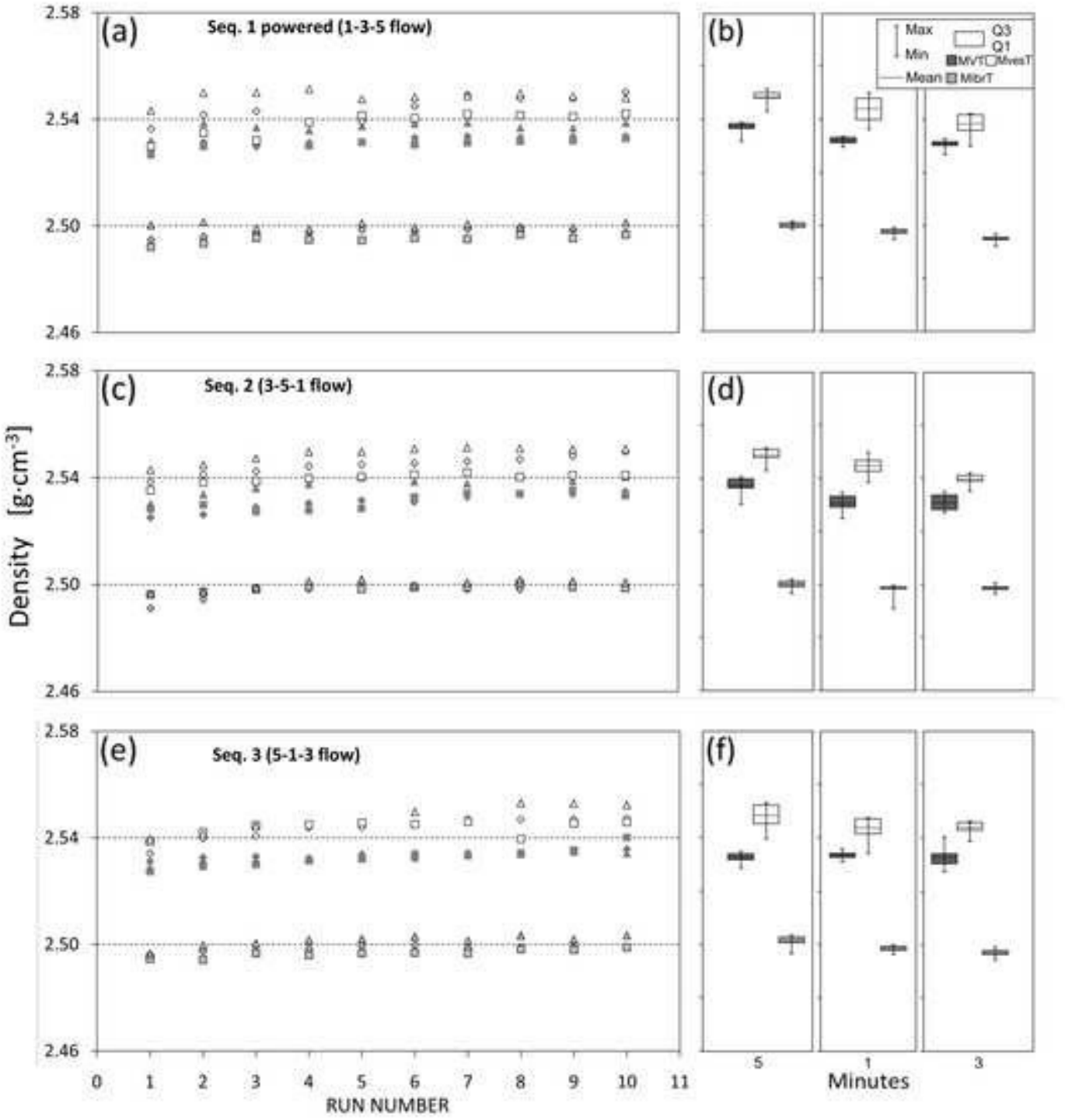
(a)
Seq. 1 powered (1-3-5 flow)
(b)
(c)
Seq. 2 (3-5-1 flow)
(d)
(e)
Seq. 3 (5-1-3 flow)
(f)
Max
Min
Mean
Q3
Q1
MbrT
MvesT
Density [g·cm-3]
2.58
2.54
2.50
2.46
0
1
2
3
4
5
6
7
8
9
10
11
RUN NUMBER
5
1
3
Minutes

Figure 7

g

Click here to access/download;Figure(s);Fig.5.jp

Figure 8

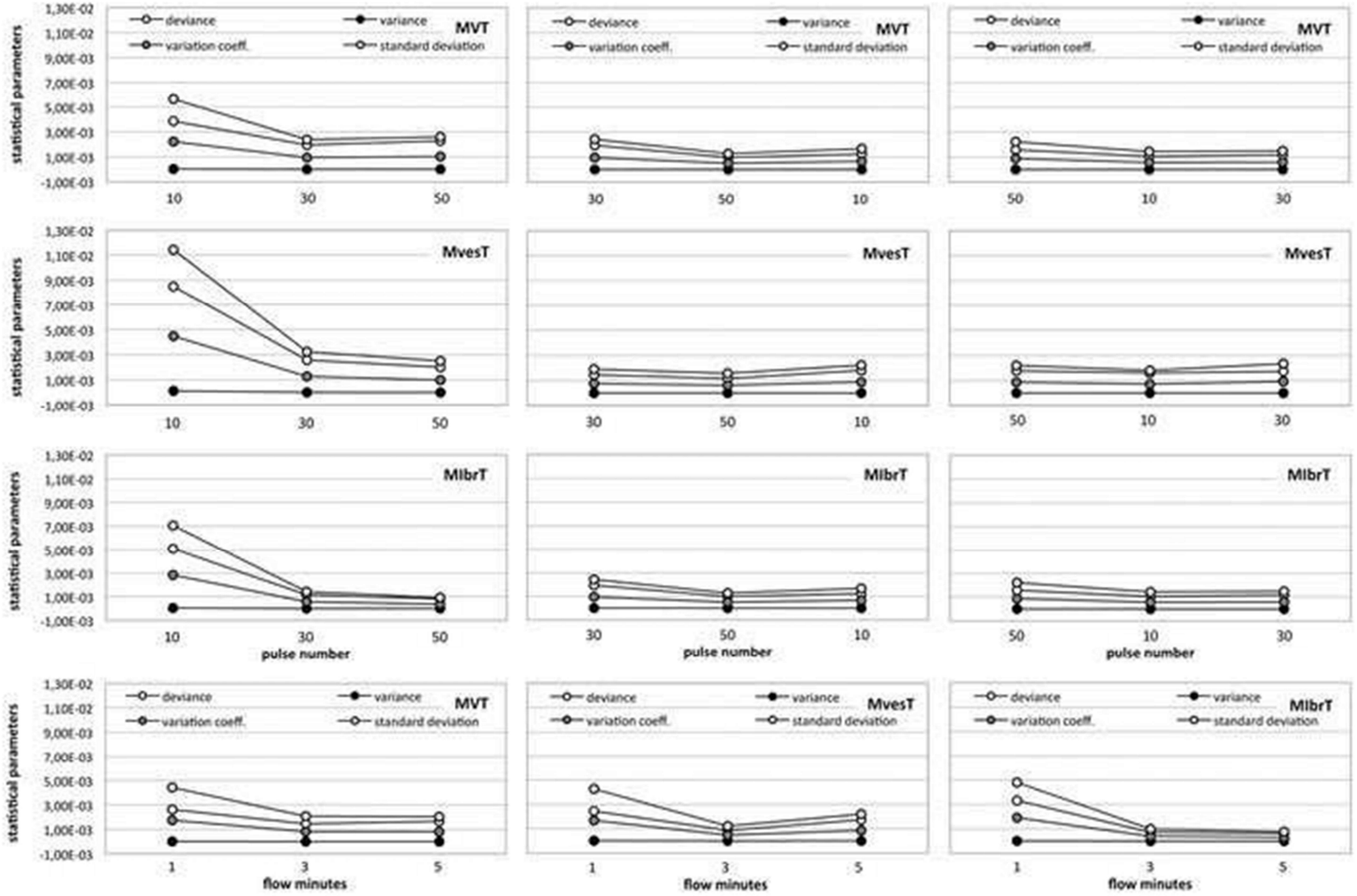
deviance
variance
variation coeff.
standard deviation
MVT
MvesT
MIbrT
statistical parameters
1,30E-02
1,10E-02
9,00E-03
7,00E-03
5,00E-03
3,00E-03
1,00E-03
-1,00E-03
10
30
50
pulse number
1
3
5
flow minutes

Figure 9

g

Click here to access/download;Figure(s);Fig.6.jp

Figure 10

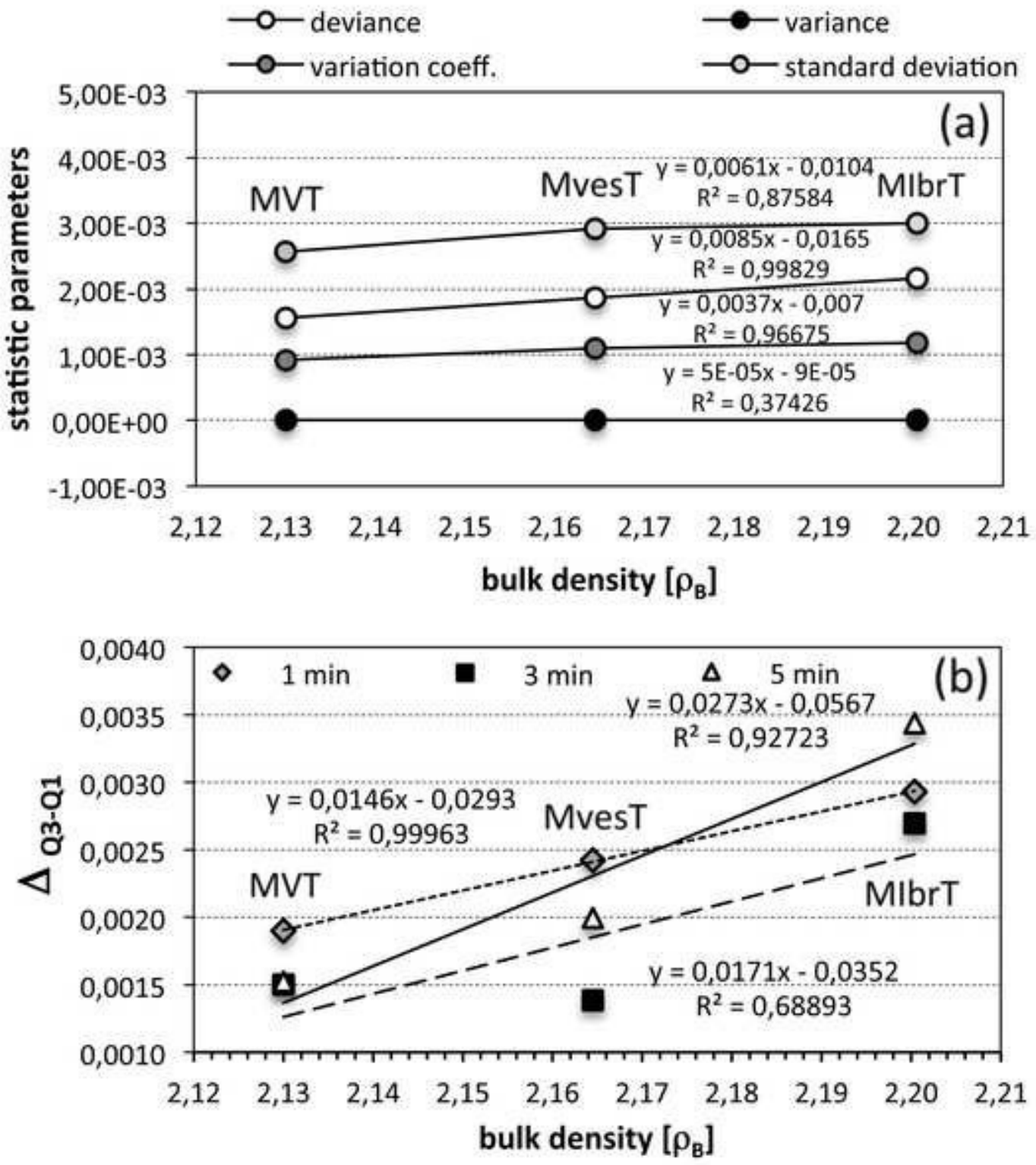
deviance
variance
variation coeff.
standard deviation
(a)
statistic parameters
5,00E-03
4,00E-03
3,00E-03
2,00E-03
1,00E-03
0,00E+00
-1,00E-03
MVT
MvesT
MIbrT
y = 0,0061x - 0,0104
R² = 0,87584
y = 0,0085x - 0,0165
R² = 0,99829
y = 0,0037x - 0,007
R² = 0,96675
y = 5E-05x - 9E-05
R² = 0,37426
2,12
2,13
2,14
2,15
2,16
2,17
2,18
2,19
2,20
2,21
bulk density [ρB]
(b)
1 min
3 min
5 min
Δ Q3-Q1
0,0040
0,0035
0,0030
0,0025
0,0020
0,0015
0,0010
y = 0,0273x - 0,0567
R² = 0,92723
y = 0,0146x - 0,0293
R² = 0,99963
MvesT
MVT
MIbrT
y = 0,0171x - 0,0352
R² = 0,68893
2,12
2,13
2,14
2,15
2,16
2,17
2,18
2,19
2,20
2,21
bulk density [ρB]

Figure 11

g

Click here to access/download;Figure(s);Fig.7.jp

Figure 12

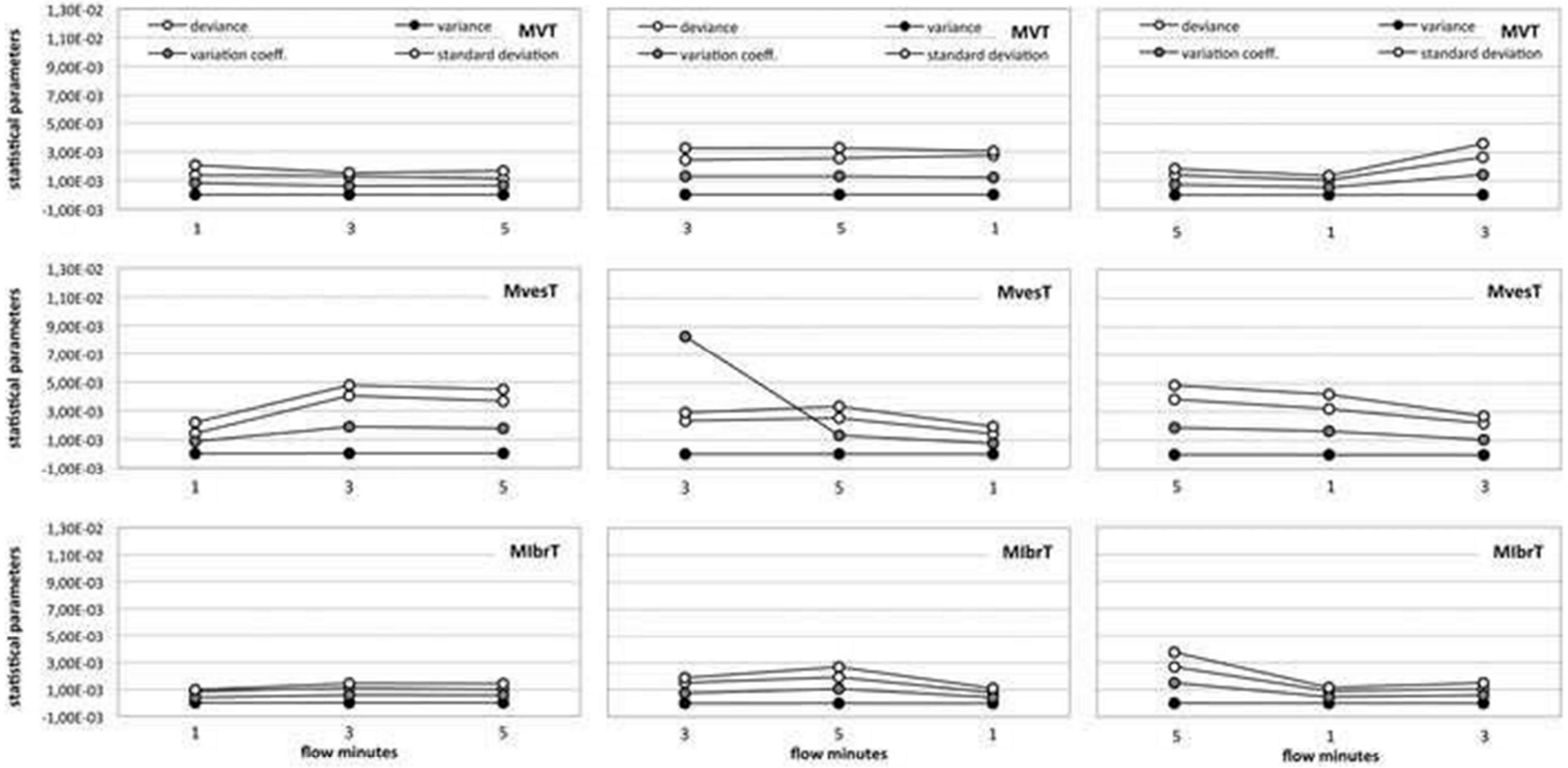
statistical parameters
1,30E-02
1,10E-02
9,00E-03
7,00E-03
5,00E-03
3,00E-03
1,00E-03
-1,00E-03
deviance
variance
variation coeff.
standard deviation
MVT
MvesT
MlbrT
1
3
5
flow minutes

Figure 13

g

Click here to
access/download;Figure(s);Fig.8.jp

Figure 14

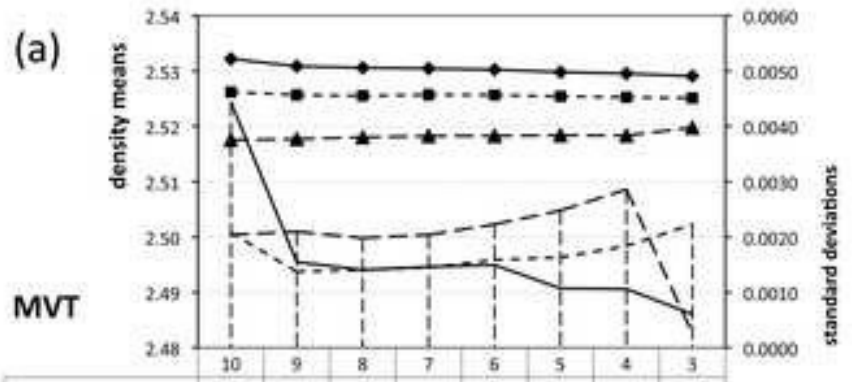

	10	9	8	7	6	5	4	3
density 1 min	2.5322	2.5309	2.5306	2.5304	2.5303	2.5298	2.5295	2.5291
density 3 min	2.5262	2.5257	2.5255	2.5257	2.5257	2.5254	2.5252	2.5251
density 5 min	2.5175	2.5177	2.5180	2.5182	2.5183	2.5184	2.5183	2.5198
st. dev. 1 min	0.0044	0.0015	0.0014	0.0015	0.0015	0.0011	0.0011	0.0006
st. dev. 3 min	0.00208	0.00137	0.00140	0.00145	0.00159	0.00163	0.00184	0.00223
st. dev. 5 min	0.00204	0.00210	0.00198	0.00204	0.00223	0.00248	0.00286	0.00026

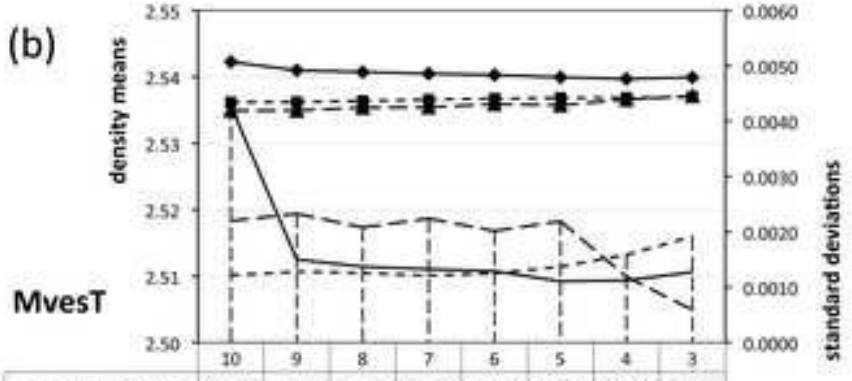

	10	9	8	7	6	5	4	3
density 1 min	2.5423	2.5410	2.5407	2.5405	2.5403	2.5399	2.5397	2.5399
density 3 min	2.5362	2.5362	2.5364	2.5366	2.5367	2.5368	2.5369	2.5370
density 5 min	2.5349	2.5349	2.5354	2.5354	2.5359	2.5357	2.5366	2.5371
st. dev. 1 min	0.0043	0.0015	0.0014	0.0013	0.0013	0.0011	0.0011	0.0013
st. dev. 3 min	0.0012	0.0013	0.0013	0.0012	0.0013	0.0014	0.0016	0.0019
st. dev. 5 min	0.0022	0.0023	0.0021	0.0022	0.0020	0.0022	0.0012	0.0006

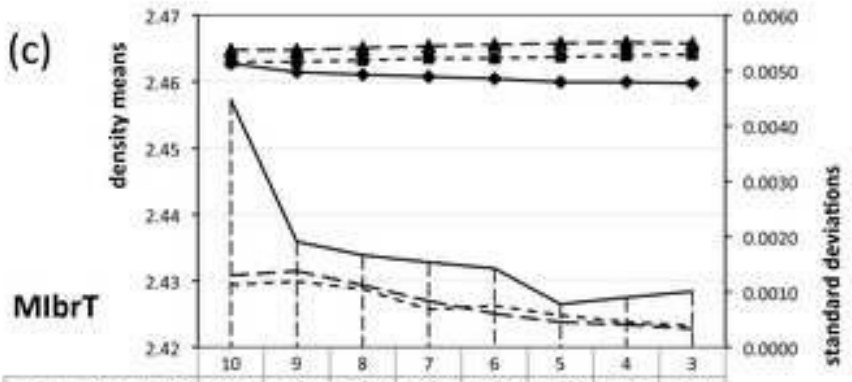

	10	9	8	7	6	5	4	3
density 1 min	2.4627	2.4614	2.4611	2.4608	2.4604	2.4599	2.4599	2.4597
density 3 min	2.4629	2.4630	2.4632	2.4635	2.4635	2.4637	2.4639	2.4641
density 5 min	2.4648	2.4648	2.4651	2.4654	2.4656	2.4658	2.4659	2.4658
st. dev. 1 min	0.0045	0.0019	0.0017	0.0015	0.0014	0.0008	0.0009	0.0010
st. dev. 3 min	0.0011	0.0012	0.0011	0.0007	0.0008	0.0006	0.0005	0.0004
st. dev. 5 min	0.0013	0.0014	0.0011	0.0008	0.0006	0.0005	0.0004	0.0003

Table 1

Bulk rock samples			
	Pulse-mode purge		
Sequence number	1st	2nd	3rd
Pulse cycles	10 - 30 - 50	30 - 50 - 10	50 - 10 - 30
	Flow-mode purge		
Sequence number	1st	n.d.	n.d.
Minute cycles	1' - 3' - 5'	n.d.	n.d.
Powered samples			
	Flow-mode purge		
Sequence number	1st	2nd	3rd
Minute cycles	1 - 3 - 5	3 - 5 - 1	5 - 1 - 3

Table 1. Measurement strategy used for the sample analysis, organized in ten runs for each performed cycle with pulses or flow purge mode, and three cycles for each performed sequence with three different pulse numbers (10, 30, 50) or flow time (1, 3, 5 minutes). n.d. = not determined.

Table 2

Rock	MVT			MvesT			MIbrT		
	pulse			pulse			pulse number		
Runs	(10)	(30)	(50)	(10)	(30)	(50)	(10)	(30)	(50)
1	2.5507	2.5222	2.5196	2.5772	2.5356	2.5332	2.5015	2.4718	2.4689
2	2.5427	2.5268	2.5246	2.5573	2.5372	2.5376	2.4902	2.4709	2.4704
3	2.5379	2.5286	2.523	2.5552	2.5360	2.5335	2.4872	2.4740	2.4694
4	2.5394	2.5278	2.5231	2.5418	2.5445	2.5367	2.4857	2.4750	2.4688
5	2.5365	2.5273	2.5231	2.5466	2.5429	2.5386	2.4838	2.4730	2.4706
6	2.5376	2.5262	2.5199	2.5442	2.5406	2.5336	2.4821	2.4727	2.4700
7	2.5351	2.5276	2.5168	2.5418	2.5372	2.5310	2.4803	2.4721	2.4707
8	2.5356	2.5281	2.5194	2.5421	2.5383	2.5317	2.4806	2.4748	2.4688
9	2.5313	2.5238	2.5243	2.5408	2.5345	2.5336	2.4770	2.4716	2.4703
10	2.5317	2.5225	2.5196	2.5438	2.5394	2.5333	2.4795	2.4716	2.4680
□□	**2.5379**	**2.5261**	**2.5213**	**2.5491**	**2.5386**	**2.5343**	**2.4848**	**2.4728**	**2.4696**
□□	5.64E-03	2.38E-03	2.60E-03	1.14E-02	3.24E-03	2.51E-03	7.07E-03	1.43E-03	9.35E-04
□□	3.18E-05	5.64E-06	6.76E-06	1.31E-04	1.05E-05	6.29E-06	5.00E-05	2.03E-06	8.74E-07
□□	3.86E-03	1.95E-03	2.28E-03	8.49E-03	2.58E-03	2.01E-03	5.09E-03	1.16E-03	8.10E-04
R	1.94E-02	6.40E-03	7.80E-03	3.64E-02	1.00E-02	7.60E-03	2.45E-02	4.10E-03	2.70E-03
□□	2.22E-03	9.40E-04	1.03E-03	4.49E-03	1.28E-03	9.90E-04	2.84E-03	5.76E-04	3.79E-04
			-04	C		-04 2.50E	-04		-05
1.05E-04	1.15E	5.07E	1.44E-04	1.11E-04	-04	3.13E	6.32E-05	4.15E	
Q_1	2.5352	2.5244	2.5196	2.5419	2.5363	2.5332	2.4804	2.4717	2.4688
Q_3	2.5390	2.5278	2.5231	2.5531	2.5403	2.5359	2.4868	2.4738	2.4704
□$_{Q3-Q1}$	0.0038	0.0034	0.0035	0.0112	0.0040	0.0027	0.0065	0.0021	0.0016
m	2.5371	2.5271	2.5215	2.5440	2.5378	2.5336	2.4830	2.4724	2.4697
k	2.3866	-0.9486	-1.1009	3.8973	-0.4343	-0.6594	3.0108	-1.0642	-1.2930
□$_1$□	1.3094	-0.8561	-0.3030	1.9563	0.6885	0.6657	1.5860	0.5501	-0.3372

Runs	(30)	(50)	(10)	(30)	(50)	(10)	(30)	(50)	(10)	(30)	(50)	(10)
1	2.5336	2.526	2.5203	2.5428	2.5394	2.5428	2.4775	2.4677	2.4663			
2	2.5291	2.5245	2.5236		2.5485	2.5423	2.5435		2.4770	2.4680	2.4695	
3	2.5313	2.5242	2.5237		2.5486	2.5407	2.5402		2.4759	2.4720	2.4664	
4	2.5311	2.5257	2.5248		2.5459	2.5424	2.5391		2.4754	2.4705	2.4691	
5	2.5306	2.526	2.5259		2.5475	2.5401	2.5395		2.4752	2.4690	2.4657	
6	2.532	2.524	2.5239		2.5440	2.5402	2.5424		2.4771	2.4651	2.4668	
7	2.5299	2.525	2.5252		2.5463	2.5400	2.5425		2.4751	2.4709	2.4680	
8	2.526	2.5224	2.5221		2.5449	2.5420	2.5408		2.4734	2.4663	2.4674	
9	2.5267	2.5242	2.5233		2.5447	2.5410	2.5365		2.4727	2.4653	2.4690	
10	2.5277	2.5226	2.522		2.5459	2.5372	2.5387		2.4761	2.4681	2.4663	
□□	**2.5298**	**2.5245**	**2.5235**		**2.5459**	**2.5405**	**2.5406**		**2.4755**	**2.4683**	**2.4675**	
□□	2.42E-03	1.27E-03	1.67E-03		1.90E-03	1.56E-03	2.22E-03		1.56E-03	2.35E-03	1.37E-03	
□□	5.87E-06	1.62E-06	2.78E-06		3.60E-06	2.44E-06	4.91E-06		2.42E-06	5.50E-06	1.87E-06	
□□	1.94E-03	9.80E-04	1.24E-03		1.45E-03	1.15E-03	1.80E-03		1.18E-03	1.85E-03	1.16E-03	
R	7.60E-03	3.60E-03	5.60E-03		5.80E-03	5.20E-03	7.00E-03		4.80E-03	6.90E-03	3.80E-03	
□□	9.58E-04	5.05E-04	6.61E-04		7.46E-04	6.15E-04	8.72E-04		6.29E-04	9.50E-04	5.55E-04	
			-05		C		-04 1.07E		-05		-05	
5.65E-05	7.40E	8.42E	6.93E-05	9.82E-05	-05	6.90E	1.04E-04	6.07E				
Q_1	2.5281	2.5241	2.5224		2.5448	2.5400	2.5392		2.4751	2.4667	2.4663	
Q_3	2.5313	2.5255	2.5246	2.5472	2.5418	2.5425	2.4768	2.4701	2.4688			
□$_{Q3-Q1}$	0.0032	0.0015	0.0022	0.0025	0.0017	0.0033	0.0017	0.0035	0.0024			
m	2.5303	2.5244	2.5237	2.5459	2.5405	2.5405	2.4757	2.4681	2.4671			
k	-0.7856	-0.7245	0.0833	-0.7449	1.2033	-0.5366	-0.2038	-1.0270	-1.5294			
□$_1$□	-0.2214	-0.3983	-0.4905	0.0217	-0.8465	-0.4190	-0.6684	0.1366	0.3879			

Runs	(50)	(10)	(30)	(50)	(10)	(30)	(50)	(10)	(30)
1	2.5349	2.5258	2.5239	2.5456	2.5399	2.5378	2.4717	2.4703	2.4663
2	2.5322	2.5231	2.5203	2.5499	2.5419	2.5380	2.4731	2.4697	2.4680
3	2.5308	2.523	2.5191	2.5453	2.5437	2.5404	2.4727	2.4719	2.4683
4	2.5307	2.5228	2.5212	2.5455	2.5424	2.5426	2.4739	2.4706	2.4666
5	2.5322	2.5219	2.5223	2.5436	2.5432	2.5357	2.4714	2.4700	2.4674
6	2.5281	2.5218	2.5195	2.5431	2.5392	2.5392	2.4723	2.4712	2.4688
7	2.5303	2.5216	2.522	2.5475	2.5402	2.5368	2.4731	2.4675	2.4689
8	2.5271	2.5211	2.5196	2.5463	2.5387	2.5361	2.4727	2.4682	2.4677
9	2.5304	2.5216	2.5202	2.5484	2.5423	2.5348	2.4725	2.4686	2.4675
10	2.5291	2.5208	2.5206	2.5485	2.5395	2.5381	2.4732	2.4689	2.4681
□□	2.5306	2.5224	2.5209	2.5464	2.5411	2.5380	2.4727	2.4697	2.4678
□□	2.22E-03	1.44E-03	1.49E-03	2.19E-03	1.80E-03	2.33E-03	7.37E-04	1.39E-03	8.51E-04
□□	4.95E-06	2.08E-06	2.23E-06	4.81E-06	3.24E-06	5.44E-06	5.43E-07	1.92E-06	7.25E-07
□□	1.58E-03	1.06E-03	1.18E-03	1.76E-03	1.60E-03	1.71E-03	5.48E-04	1.11E-03	6.60E-04
R	7.80E-03	5.00E-03	4.80E-03	6.80E-03	5.00E-03	7.80E-03	2.50E-03	4.40E-03	2.60E-03
□□	8.79E-04	5.71E-04	5.93E-04	8.61E-04	7.08E-04	9.19E-04	2.98E-04	5.61E-04	3.45E-04

Table 3

				-05			-05			-05
				C		-05	9.86E	-05		-05
6.39E-05	6.62E		9.72E	7.98E-05	1.03E-04	-05	3.27E	6.15E-05	3.78E	
Q_1	2.5294	2.5216	2.5198	2.5454	2.5396	2.5363	2.4724	2.4687	2.4674	
Q_3	2.5319	2.5230	2.5218	2.5482	2.5424	2.5389	2.4731	2.4705	2.4683	Δ_{Q3-Q1}
0.0025	0.0014	0.0020	0.0028	0.0028	0.0026	0.0008	0.0019	0.0008	**m**	2.5306
2.5219	2.5205	2.5460	2.5411	2.5379	2.4727	2.4699	2.4679	**k**	0.5750	3.3161
0.3238	-0.8450	-1.7129	0.4060	0.0419	-0.8132	-0.4614				
Δ_1	0.3592	1.6284	0.8981	0.0646	0.0964	0.7301	-0.2436	-0.0184	-0.4322	

Table 2. Real density values on ten run cycles and main statistic parameters of MVT, MvesT and MIbrT rock specimens determined on pulse purge mode with sequence of (10, 30, 50), (30, 10, 50) and (50, 10, 30) pulses. Legend: □□= average of real density; □ = standard deviation; □² = variance; □ = deviance; R = maximum range of real density; □ = variation coefficient; C = confidence interval; Q_1 = 1° quartile of statistic distribution of ten values; Q_3 = 3° quartile; Δ_{Q3-Q1} = difference between 1st and 3rd quartile; m = median (Q_2); k = kurtosis coefficient of Pearson; □□= asymmetry index of Fischer (or coefficient of skewness).

Rock sample	MVT			MvesT			MIbrT		
		flow minutes			flow minutes		flow minutes		
Runs	**(1)**	**(3)**	**(5)**	**(1)**	**(3)**	**(5)**	**(1)**	**(3)**	**(5)**
1	2.5441	2.5308	2.5161	2.5537	2.5358	2.5347	2.5074	2.4639	2.4655
2	2.5330	2.5268	2.5151	2.5431	2.5349	2.5315	2.4990	2.4607	2.4633
3	2.5315	2.5245	2.5165	2.5422	2.5350	2.5350	2.4960	2.4621	2.4637
4	2.5316	2.5258	2.5179	2.5419	2.5357	2.5325	2.4935	2.4622	2.4642
5	2.5326	2.5269	2.5178	2.5420	2.5362	2.5369	2.4931	2.4641	2.4646
6	2.5308	2.5261	2.5186	2.5409	2.5368	2.5323	2.4928	2.4628	2.4653
7	2.5309	2.5256	2.5141	2.5391	2.5365	2.5350	2.4941	2.4620	2.4646
8	2.5296	2.5247	2.5195	2.5412	2.5352	2.5372	2.4915	2.4619	2.4651
9	2.5291	2.5275	2.5200	2.5398	2.5367	2.5377	2.4916	2.4627	2.4655
10	2.5284	2.5231	2.5197	2.5387	2.5390	2.5365	2.4937	2.4625	2.4653
□□	**2.5322**	**2.5262**	**2.5175**	**2.5423**	**2.5362**	**2.5349**	**2.4953**	**2.4625**	**2.4647**
□□	4.43E-03	2.08E-03	2.04E-03	4.27E-03	1.22E-03	2.20E-03	4.80E-03	9.89E-04	7.71E-04
□□	1.97E-05	4.32E-06	4.16E-06	1.83E-05	1.48E-06	4.82E-06	2.30E-05	9.77E-07	5.95E-07
□□	2.63E-03	1.46E-03	1.67E-03	2.45E-03	8.67E-04	1.73E-03	3.32E-03	7.18E-04	6.24E-04
R	1.57E-02	7.68E-03	5.99E-03	1.50E-02	4.16E-03	6.13E-03	1.59E-02	3.37E-03	2.27E-03
□□	1.75E-03	8.23E-04	8.11E-04	1.68E-03	4.80E-04	8.66E-04	1.92E-03	4.01E-04	3.13E-04
C	-04	9.22E-05	9.05E-05	1.89E-04	5.39E-05	9.74E-05	2.13E-04	4.38E-05	3.42E-05
Q_1	97E 2.5299	2.5249	2.5162	2.5401	2.5353	2.5331	2.4929	2.4620	2.4643
Q_3	2.5324	2.5269	2.5193	2.5422	2.5366	2.5368	2.4955	2.4627	2.4653
Δ_{Q3-Q1}	0.0024	0.0020	0.0031	0.0021	0.0013	0.0037	0.0026	0.0008	0.0009
m	2.5312	2.5259	2.5179	2.5416	2.5360	2.5350	2.4936	2.4624	2.4648
k	7.2351	2.2213	-0.9788	7.2120	2.9076	-1.3438	4.8087	0.4665	-0.4714
□$_1$□	2.5334	1.0116	-0.4213	2.5202	1.4440	-0.3522	2.1284	0.1654	-0.7726

Table 3. Real density values on ten run series and main statistic parameters of MVT, MvesT and MIbrT rock specimens determined on flow purge mode with sequence of (1, 3, 5) minutes. Legend as in Table 2.

Powdered sample	MVT			MvesT			MIbrT		
		flow minutes			flow minutes		flow minutes		
Runs	**(1)**	**(3)**	**(5)**	**(1)**	**(3)**	**(5)**	**(1)**	**(3)**	**(5)**
1	2.5318	2.5297	2.5268	2.5432	2.5364	2.5299	2.5003	2.4948	2.4921
2	2.5385	2.5314	2.5299	2.5499	2.5416	2.5350	2.5015	2.4959	2.4935
3	2.5369	2.5298	2.5307	2.5500	2.5431	2.5321	2.4991	2.4969	2.4955
4	2.5359	2.5312	2.5301	2.5513	2.5391	2.5389	2.4987	2.4978	2.4949
5	2.5374	2.5316	2.5314	2.5476	2.5393	2.5415	2.5011	2.4985	2.4946
6	2.5384	2.533	2.5305	2.5483	2.5450	2.5405	2.4995	2.4981	2.4955
7	2.5387	2.5336	2.5312	2.5488	2.5491	2.5420	2.5007	2.4989	2.4951

Table 4

8	2.5368	2.5331	2.5318	2.5497	2.5479	2.5415	2.4996	2.4994	2.4967
9	2.5367	2.5334	2.532	2.5487	2.5478	2.5410	2.4995	2.4986	2.4954
10	2.5386	2.5337	2.5329	2.5480	2.5502	2.5421	2.5011	2.4975	2.4968
□□	**2.5370**	**2.5321**	**2.5307**	**2.5486**	**2.5440**	**2.5385**	**2.5001**	**2.4976**	**2.4950**
□□	2.06E-03	1.52E-03	1.66E-03	2.18E-03	4.78E-03	4.48E-03	9.60E-04	1.42E-03	1.40E-03
□²□	4.24E-06	2.32E-06	2.75E-06	4.75E-06	2.28E-05	2.01E-05	9.21E-07	2.03E-06	1.96E-06
□□	1.35E-03	1.31E-03	1.13E-03	1.42E-03	4.05E-03	3.67E-03	8.30E-04	1.09E-03	9.88E-04
R	6.90E-03	4.00E-03	6.10E-03	6.50E-03	1.38E-02	1.22E-02	2.40E-03	4.60E-03	4.70E-03
□□	8.12E-04	6.02E-04	6.55E-04	8.56E-04	1.88E-03	1.77E-03	3.84E-04	5.70E-04	5.61E-04
C	-05	6.75E-05	7.35E-05	9.67E-05	2.12E-04	1.99E-04	4.26E-05	6.31E-05	6.21E-05
Q_1	14E	2.5313	2.5302	2.5481	2.5399	2.5360	2.4995	2.4971	2.4947
	2.5367								
Q_3	2.5385	2.5333	2.5317	2.5499	2.5479	2.5415	2.5010	2.4986	2.4955
□$_{Q3-Q1}$	0.0017	0.0021	0.0015	0.0018	0.0080	0.0055	0.0015	0.0015	0.0008
m	2.5372	2.5323	2.5310	2.5488	2.5441	2.5408	2.5000	2.4980	2.4953
k	4.6430	-1.2832	3.3415	4.2254	-1.4112	-0.1837	-1.4795	0.3389	1.0930
□$_1$□	-1.9590	-0.4973	-1.4533	-1.6927	-0.2011	-1.1522	0.0657	-0.9388	-0.8764
Runs	**(3)**	**(5)**	**(1)**	**(3)**	**(5)**	**(1)**	**(3)**	**(5)**	**(1)**
1	2.5302	2.5251	2.5283	2.5429	2.5384	2.5353	2.4965	2.4911	2.4963
2	2.5337	2.5262	2.5299	2.5447	2.5412	2.5382	2.4971	2.4944	2.4974
3	2.536	2.5289	2.5273	2.5472	2.5423	2.5386	2.4989	2.4987	2.4982
4	2.5376	2.5304	2.5278	2.5496	2.5442	2.5397	2.5011	2.4984	2.4991
5	2.5401	2.5315	2.5285	2.5497	2.5449	2.5404	2.5019	2.4993	2.4983
6	2.5385	2.531	2.5327	2.5508	2.5453	2.5411	2.4996	2.4992	2.4990
7	2.5377	2.5328	2.5341	2.5512	2.5460	2.5419	2.5007	2.4983	2.4990
8	2.5404	2.5337	2.5339	2.5509	2.5468	2.5403	2.5016	2.4983	2.5004
9	2.5387	2.5339	2.5352	2.5506	2.5481	2.5409	2.5012	2.4989	2.4991
10	2.5403	2.5348	2.5333	2.5507	2.5497	2.5410	2.5008	2.4992	2.4987
□□	**2.5373**	**2.5308**	**2.5311**	**2.5488**	**2.5447**	**2.5397**	**2.4999**	**2.4976**	**2.4986**
□□	3.25E-03	3.27E-03	3.03E-03	2.92E-03	3.35E-03	1.93E-03	1.88E-03	2.69E-03	1.11E-03
□²□	1.06E-05	1.07E-05	9.16E-06	8.52E-06	1.12E-05	3.73E-06	3.55E-06	7.22E-06	1.22E-06
□□	2.41E-03	2.54E-03	2.74E-03	2.34E-03	2.53E-03	1.43E-03	1.53E-03	1.93E-03	8.00E-04
R	1.02E-02	9.70E-03	5.80E-03	8.00E-03	1.13E-02	6.60E-03	5.10E-03	8.20E-03	4.10E-03
□□	1.28E-03	1.29E-03	1.20E-03	8.30E-03	1.32E-03	7.61E-04	7.54E-04	1.08E-03	4.43E-04
C	-04	1.45E-04	1.34E-04	1.29E-04	1.49E-04	8.57E-05	8.35E-05	1.19E-04	4.91E-05
Q_1	44E	2.5293	2.5284	2.5478	2.5428	2.5389	2.4991	2.4983	2.4982
	2.5364								
Q_3	2.5398	2.5335	2.5338	2.5508	2.5466	2.5410	2.5012	2.4991	2.4991
□$_{Q3-Q1}$	0.0033	0.0042	0.0054	0.0030	0.0038	0.0021	0.0021	0.0008	0.0008
m	2.5381	2.5313	2.5313	2.5502	2.5451	2.5404	2.5008	2.4986	2.4989
k	1.4767	-0.5538	-2.0196	0.5440	0.0523	2.3339	-0.2882	3.5801	1.3876
□$_1$□	-1.3298	-0.6844	0.0028	-1.3429	-0.4723	-1.4652	-0.9978	-2.0434	-0.6269
Runs	**(5)**	**(1)**	**(3)**	**(5)**	**(1)**	**(3)**	**(5)**	**(1)**	**(3)**
1	2.5287	2.5311	2.5274	2.5396	2.5342	2.5387	2.4965	2.4962	2.4946
2	2.5317	2.5326	2.5293	2.5414	2.5399	2.5422	2.4997	2.4975	2.4942
3	2.5315	2.533	2.53	2.5443	2.5407	2.5447	2.5004	2.4973	2.4967
4	2.5319	2.5324	2.5315	2.5483	2.5440	2.5450	2.5017	2.4984	2.4960
5	2.5323	2.5338	2.5323	2.5491	2.5441	2.5457	2.5021	2.4996	2.4967
6	2.5326	2.5342	2.5336	2.5497	2.5452	2.5451	2.5030	2.4999	2.4969
7	2.5342	2.5342	2.5334	2.5516	2.5469	2.5460	2.5015	2.4986	2.4967
8	2.534	2.5341	2.5342	2.5530	2.5470	2.5396	2.5033	2.4990	2.4982
9	2.5349	2.5347	2.5354	2.5529	2.5469	2.5455	2.5020	2.4992	2.4980
10	2.5342	2.5358	2.5402	2.5524	2.5473	2.5459	2.5034	2.4991	2.4989
□□	**2.5326**	**2.5336**	**2.5327**	**2.5482**	**2.5436**	**2.5438**	**2.5004**	**2.4985**	**2.4967**
□□	1.83E-03	1.34E-03	3.58E-03	4.86E-03	4.22E-03	2.71E-03	3.74E-03	1.16E-03	1.49E-03
□²□	3.35E-06	1.79E-06	1.28E-05	2.36E-05	1.78E-05	7.32E-06	1.40E-05	1.34E-06	2.22E-06
□□	1.38E-03	1.05E-03	2.63E-03	3.88E-03	3.21E-03	2.20E-03	2.68E-03	9.04E-04	1.05E-03
R	6.20E-03	4.70E-03	1.28E-02	1.34E-02	1.31E-02	7.30E-03	6.90E-03	3.70E-03	4.70E-03
□□	7.23E-04	5.28E-04	1.42E-03	1.91E-03	1.66E-03	1.06E-03	1.50E-03	4.62E-04	5.97E-04
C	-05	5.93E-05	1.59E-04	2.16E-04	1.87E-04	1.20E-04	1.66E-04	5.12E-05	6.60E-05
Q_1	12E	2.5327	2.5304	2.5453	2.5415	2.5428	2.4999	2.4977	2.4962
	2.5318								
Q_3	2.5342	2.5342	2.5341	2.5522	2.5469	2.5457	2.5028	2.4992	2.4977
□$_{Q3-Q1}$	0.0024	0.0015	0.0037	0.0069	0.0054	0.0028	0.0029	0.0014	0.0015
m	2.5325	2.5340	2.5329	2.5494	2.5447	2.5451	2.5019	2.4988	2.4967
k	1.0690	0.2420	1.1797	-0.6730	1.6277	0.1108	3.0004	0.0703	-0.3604
□$_1$□	-0.8741	-0.3214	0.6815	-0.8420	-1.3822	-1.2791	-1.7703	-0.8476	-0.3531

Table 4. Real density values on ten run series and main statistic parameters of MVT, MvesT and MIbrT powdered specimens determined on flow purge mode with sequence of (1, 3, 5), (3, 5, 1) and (5, 1, 3) minutes. Legend as in Table 2.

Table 5

Rock sample	*a*E	*r*E %	*a*E	*r*E %	*a*E	*r*E %
Pulse number	**(10)**		**(30)**		**(50)**	
MVT	1.29E-02	5.06E-01	3.89E-03	1.54E-01	4.54E-03	1.80E-01
MvesT	2.81E-02	1.10E+00	5.88E-03	2.32E-01	4.32E-03	1.70E-01
MIbrT	1.67E-02	6.72E-01	2.25E-03	9.10E-02	1.59E-03	6.44E-02
Pulse number	**(30)**		**(50)**		**(10)**	
MVT	3.80E-03	1.50E-01	2.06E-03	8.16E-02	2.42E-03	9.59E-02
MvesT	3.11E-03	1.22E-01	3.33E-03	1.31E-01	2.90E-03	1.14E-01
MIbrT	2.84E-03	1.15E-01	3.71E-03	1.50E-01	2.19E-03	8.88E-02
Pulse number	**(50)**		**(10)**		**(30)**	
MVT	4.32E-03	1.71E-01	3.45E-03	1.37E-01	3.03E-03	1.20E-01
MvesT	3.53E-03	1.39E-01	2.60E-03	1.02E-01	4.65E-03	1.83E-01
MIbrT	1.26E-03	5.10E-02	2.21E-03	8.95E-02	1.46E-03	5.92E-02
Flow minutes	**(1)**		**(3)**		**(5)**	
MVT	1.19E-02	4.71E-01	4.63E-03	1.83E-01	2.51E-03	9.97E-02
MvesT	1.15E-02	4.51E-01	2.86E-03	1.13E-01	2.75E-03	1.09E-01
MIbrT	1.21E-02	4.85E-01	1.60E-03	6.49E-02	8.44E-04	3.42E-02

Table 5. Absolute error (*a*E) and relative error (*r*E %) of real density values of MVT, MvesT and MIbrT rock specimens determined with helium pycnometry with pulse purge mode on the three sequences: (10, 30, 50), (30, 50, 10) and (50, 10, 30) pulses, and with flow purge mode on the sequence (1, 3, 5) minutes. Absolute error is calculated as difference between the maximum (or minimum) value and the average value (that is considered as the true density value) of ten run measurements.

Table 6

Powdered sample	*a*E	*r*E %	*a*E	*r*E %	*a*E	*r*E %
Flow minutes	**(1)**		**(3)**		**(5)**	
MVT	6.10E-03	2.40E-01	2.40E-03	9.48E-02	3.90E-03	1.54E-01
MvesT	5.40E-03	2.12E-01	7.60E-03	2.99E-01	8.60E-03	3.39E-01
MIbrT	1.41E-03	5.64E-02	2.80E-03	1.12E-01	2.90E-03	1.16E-01
Flow minutes	**(3)**		**(5)**		**(1)**	
MVT	7.10E-03	2.80E-01	5.70E-03	2.25E-01	4.10E-03	1.62E-01
MvesT	5.90E-03	2.31E-01	6.30E-03	2.48E-01	4.40E-03	1.73E-01
MIbrT	2.90E-03	1.16E-01	6.50E-03	2.60E-01	2.30E-03	9.21E-02
Flow minutes	**(5)**		**(1)**		**(3)**	
MVT	3.90E-03	1.54E-01	2.50E-03	9.87E-02	7.50E-03	2.96E-01
MvesT	8.60E-03	3.37E-01	9.40E-03	3.70E-01	5.10E-03	2.00E-01
MIbrT	3.90E-03	1.56E-01	2.30E-03	9.21E-02	2.50E-03	1.00E-01

Table 6. Absolute error (*a*E) and relative error (*r*E %) of solid density values of MVT, MvesT and MIbrT powdered specimens determined with Helium pycnometry with flow purge mode on the three sequences: (1, 3, 5), (3, 5, 1) and (5, 1, 3) minutes.